Changes in west Antarctic ice stream velocities: Observation and analysis

Ian Joughin
Jet Propulsion Laboratory, California Institute of Technology, Pasadena, California, USA

Slawek Tulaczyk
Department of Earth Sciences, University of California-Santa Cruz, Santa Cruz, California, USA

Robert Bindschadler
NASA Goddard Space Flight Center, Greenbelt, Maryland, USA

Stephen F. Price
Department of Earth and Space Sciences, University of Washington, Seattle, Washington, USA

Received 21 August 2001; revised 4 March 2002; accepted 18 April 2002; published 13 November 2002.

[1] We have produced a map of velocity covering much of the Siple Coast ice streams. The map confirms earlier estimates of deceleration on Whillans Ice Stream. Comparison with bed elevation data indicates that subglacial topography and the location of consolidated sediment play a strong role in determining the location of the tributaries feeding the ice streams. Force balance estimates based on these data indicate that the tributaries have beds nearly an order of magnitude stronger than those beneath many of the ice streams. We have used a theoretical analysis to examine the controls on fast flow. This analysis suggests that ice plains (very wide ice streams) are inherently unstable. This instability may be responsible for the current deceleration on the Ice Plain of Whillans Ice Stream and the shutdown of Ice Stream C 150 years ago. Thinning-induced reductions indriving stress may also explain some of the observed deceleration, particularly in upstream areas. The active portions of Ice Stream C coincide well with the areas where we estimate that melt should be taking place. Current topography and inferences of large thickening following a shutdown suggest the upstream migration of a stagnation front that initiated at the ice plain. Uncertainty remains about the basal conditions on Ice Stream D, while the basal resistance on Ice Stream E is large enough to ensure basal melting. *INDEX TERMS:* 1827 Hydrology: Glaciology (1863); 0933 Exploration Geophysics: Remote sensing; 1863 Hydrology: Snow and ice (1827); *KEYWORDS:* ice streams, ice sheets, Synthetic Aperture Radar Interferometry (InSAR), glaciology, Antarctica

Citation: Joughin, I., S. Tulaczyk, R. Bindschadler, and S. F. Price, Changes in west Antarctic ice stream velocities: Observation and analysis, *J. Geophys. Res.*, *107*(B11), 2289, doi:10.1029/2001JB001029, 2002.

1. Introduction

[2] Initial doubts about the stability of the West Antarctic Ice Sheet [*Mercer*, 1968] led to a large glaciological research effort aimed at better understanding the controls on fast flow and potential instabilities. The nature of the fast flow in the Siple Coast ice streams (Ice Streams A and C–F and Whillans Ice Stream) has been of particular interest, since these ice streams move at relatively fast speeds (400 m/yr) despite driving stresses at least an order of magnitude less than for typical outlet glaciers. This research has greatly improved the understanding of the dynamics of this marine ice sheet. Scenarios of catastrophic collapse in the next few centuries have been deemed less likely, though not completely ruled out [*Alley and Bindschadler*, 2001].

[3] The Siple Coast region has been the site of numerous field investigations involving collection of velocity data using both Doppler Transit and Global Positioning System (GPS) survey techniques. In addition, other sources of data have been used to infer significant temporal variability of the flow field over the last millennium [*Retzlaff and Bentley*, 1993; *Jacobel et al.*, 2000; *Fahnestock et al.*, 2000]. Despite these efforts, the velocity field of the Siple Coast ice streams has remained largely unmapped. In 1997, the RADARSAT-1 synthetic aperture radar (SAR) was maneuvered to a south-looking orientation for the first complete high-resolution (25 m) radar imaging of the entire continent [*Jezek*, 1999]. This mission lasted 30 days, and with a 24 day exact-repeat cycle, it provided 6 days of repeat coverage suitable for Satellite Radar Interferometry (SRI) estimation of ice

Copyright 2002 by the American Geophysical Union.
0148-0227/02/2001JB001029$09.00

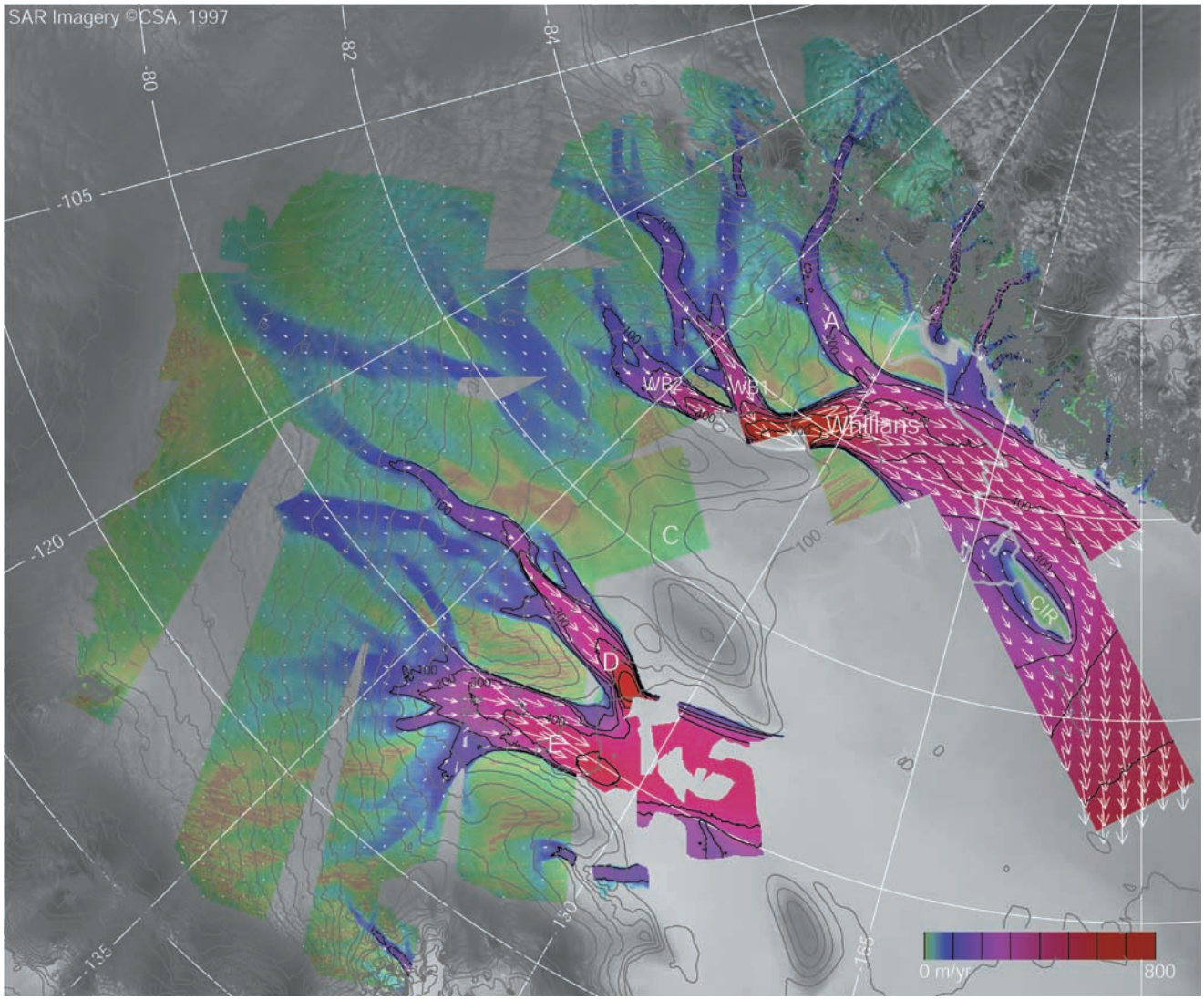

Figure 1. Velocity of Siple Coast ice streams shown on top of RAMP SAR mosaic [*Jezek*, 1999]. Speed is indicated by both color coding and 100 m/yr contours (black). Subsampled velocity vectors are shown with white arrows. Surface elevation from the RAMP DEM is shown with 100 m contours (gray). Ice streams and Crary Ice Rise (CIR) are identified with white text.

flow velocity. Several data takes from this mission were used to map velocity over much of the inland area of the ice streams, revealing a complex network of tributaries feeding the ice streams [*Joughin et al.*, 1999]. We have now processed nearly all of the available data over this area to produce a map of velocity that covers nearly the full extent of the Siple Coast ice streams. RADARSAT-1 will not be maneuvered again to a south-looking orientation. Thus, the gaps that remain await the collection of further data by some future sensor.

[4] This paper begins with a description of the data set and a comparison with previous measurements. We describe our application of standard force balance techniques [*Van der Veen*, 1999] to the ice streams and their tributaries. We conclude with an extended analysis of the velocity data in the context of tributaries, onsets, ice streams, and ice plains. In particular, we use the data in conjunction with the undrained plastic bed model [*Tulaczyk et al.*, 2000a] to investigate the stability of ice streams and ice plains.

2. Velocity Data

[5] We have derived a map (Figure 1) of ice flow velocity for the Siple Coast ice streams using a combination of conventional interferometry and speckle-tracking methods applied to RADARSAT data collected during the first Antarctic Mapping Mission (AMM-1). On the downstream areas of Ice Streams D, E, and F, the map also includes data [*Bindschadler et al.*, 1996] generated by tracking features visible in pairs of Landsat or other images. A small gap in the upper catchment of Ice Stream D was filled using GPS-derived velocities from a dense (5 km) survey grid [*Chen et al.*, 1998]. A total of 19 interferometric pairs were used to generate the velocity map, which represents the substantial augmentation of an

earlier map [*Joughin et al.*, 1999] that was based on only 4 interferometric pairs.

[6] Only a brief discussion of the velocity estimation method is included here. A detailed description of the algorithms and software used to produce the map is given by *Joughin* [2002]. Conventional interferometry relies on the phase difference between pairs of SAR images to make precise estimates of the range displacement. Under an assumption of surface-parallel flow [*Joughin et al.*, 1998; *Mohr et al.*, 1998], data from ascending and descending passes can be combined to produce a vector velocity estimate.

[7] The 24 day repeat cycle of RADARSAT provides a strong sensitivity to displacement that can result in unrecoverable unwrapped phase values in fast moving areas (i.e., >100 m/yr), where the phase becomes aliased or decorrelated. Fortunately, an alternate technique that relies on interferometric correlation has been developed [*Michel and Rignot*, 1999; *Gray et al.*, 2000] that can provide data in faster moving areas. This technique, called ''speckle tracking'', takes advantage of the ability to determine with subpixel accuracy the displacements (both across- and along-track offsets) between scenes in an interferometric pair using the sharply peaked cross correlation of SAR speckle patterns. This technique has the advantage that it can provide vector measurements of displacement using data collected along only a single satellite-track direction. The disadvantage is that it has greatly reduced resolution and accuracy compared to conventional interferometry. In some cases, particularly those where phase data are only available for a single-track direction, we use a hybrid approach in which one component of velocity is determined from phase and the other from speckle-tracked displacement estimates.

[8] The velocity is determined as the weighted sum of all input data [*Joughin*, 2002] that are available at each output grid point. To minimize error, the weights are inversely proportional to the estimated variances. Additional weighting is applied at the edges of each image (''feathering'') to reduce discontinuities at swath boundaries [*Joughin*, 2002]. The data are posted at 0.5 km intervals on a polar stereographic grid (71° standard latitude, 0° rotation). At this resolution, the interferometric phase data are well undersampled. The speckle-tracked data, however, are typically smoothed to a resolution of 1–3 km to reduce noise. As a result, the resolution of the final product varies from roughly 0.5 to 3 km.

[9] On the ice shelf, tidal effects need to be taken into account when estimating velocity. To compensate for tidal effects, we estimated the relative tidal displacement (~0.3–0.9 m) from the interferometric phase across the grounding line. This estimate was used to remove most of the effect of tidal displacement. Residual tidal effects (<10–20 cm) may result in relatively small errors (<4–8 m/yr). The interferometric phase varies rapidly at the grounding zone so that our simple correction does not apply in this region. Consequently, we have made no attempt to estimate velocity near the grounding line. As a result, the grounding zone can be seen in Figure 1 as narrow, data-free region below Ice Stream A and Whillans Ice Stream and around Crary Ice Rise. There is no similar data gap at the grounding lines of Ice Streams D and E since these velocities were determined using Landsat feature tracking.

2.1. Errors

[10] We have tracked the errors in the input data and propagated them through the velocity mosaicking and estimation process to produce a map of velocity error, which is shown in Figure 2. Because of differences in the quality, type, and amount of source data at each point, errors in the velocity map (Figure 1) have significant spatial variability.

[11] Atmospheric effects tend to dominate interferometric phase errors [*Goldstein*, 1995]. We are unable to estimate the spatial variation of this error. Based on our experience with interferometric data, we assume a uniform value of π radians for the phase error, which is an approximate upper bound. Errors in the speckle-tracked data are estimated as the sample variance determined over a small box (9×9) about each offset estimate. A plane is fit to, and subtracted from, the data in each box in an effort to remove variation due to ice motion. Despite this correction, the estimated errors are biased high by any fine-scale variability resulting from true displacements.

[12] The speckle-tracked data also have longer wavelength errors that resemble ''streaks'' running across the azimuth offset estimates, which are likely related to ionospheric effects [*Gray et al.*, 2000]. These streaks are oriented approximately with the across-track direction and have spatial variation of 1–10 km in the along-track direction. An example of streak error is visible on Ridge D/E in Figure 1. It is difficult to reliably estimate the spatial variability of these errors. Instead, we are forced to rely on an estimate of the streak variance for the entire image. The intensity of these errors can vary significantly within an image. Thus, streak errors can be significantly larger (up to ~10 m/yr) locally than the image-wide average.

[13] The largest estimated errors visible in Figure 2 coincide with the shear margins of ice streams. The estimated errors are larger in part because shear at the margins decreases interferometric correlation and degrades the quality of speckle-tracked matches. In addition, estimated errors near the margin tend to be overstated because of the difficulty in separating fine-scale motion (signal) from noise in the error estimation procedure described above.

2.2. Validation

[14] We have evaluated the quality of the velocity and velocity-error estimates using field measurements of ice velocity. Table 1 provides a comparison of our data with field measurements of velocity acquired at the locations shown in Figure 2. Although these in situ measurements were used as a source of control for the velocity map, the number of points in each data set is significantly larger than the number of degrees of freedom for the interferometric baseline fits (4 parameters per data take). Thus, the residuals provide a reasonable evaluation of the overall quality of the data.

[15] The third and fourth columns of Table 1 show for each component the standard deviations of the difference between the SRI and in situ velocity estimates. The last two columns show the averages of the corresponding estimates from the velocity error map (Figure 2). The results in Table 1

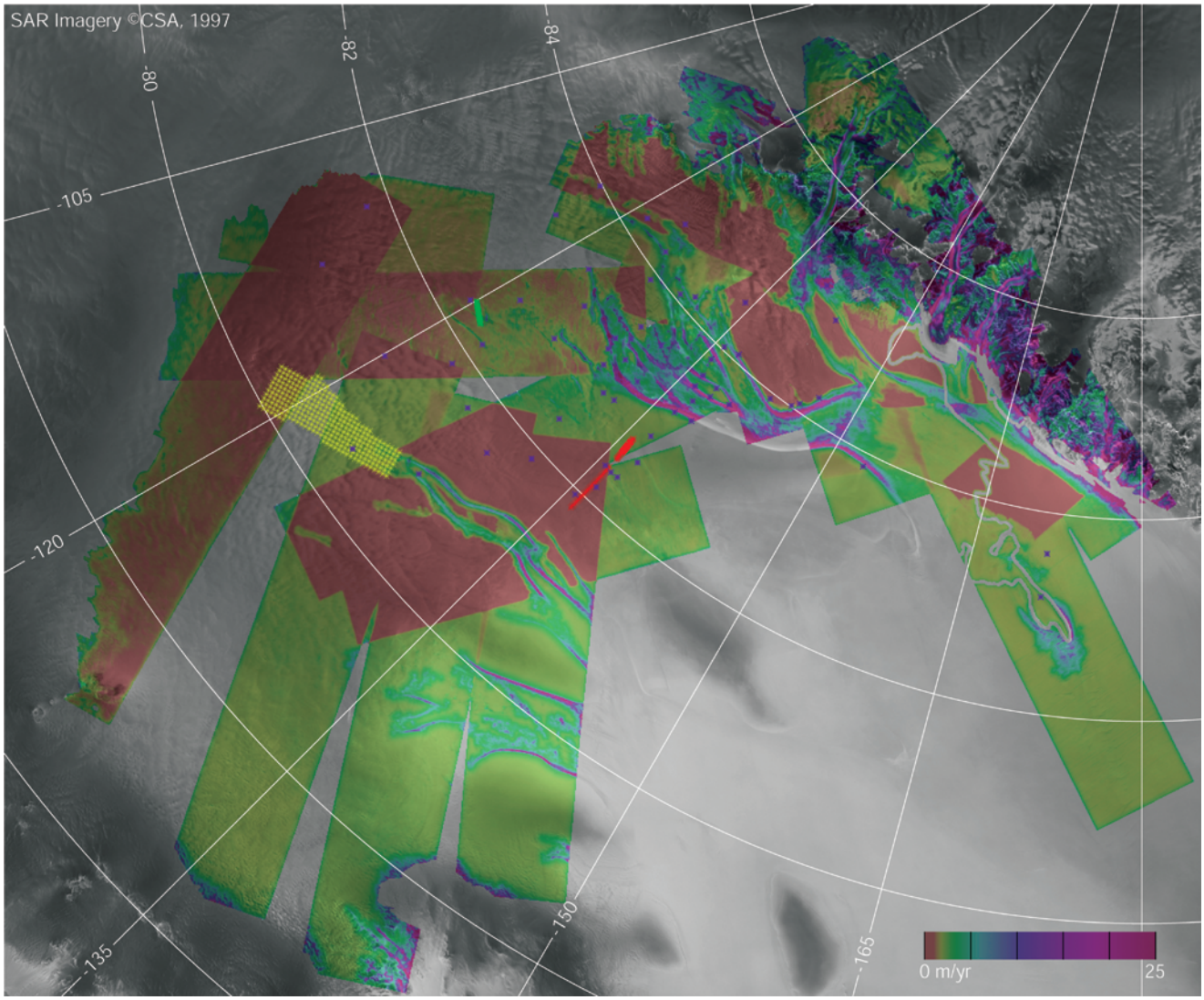

Figure 2. Magnitude of 1-sigma velocity error for velocity data shown in Figure 1.

exclude points where the magnitude of the velocity difference is greater than 15 m/yr. These points are assumed to be anomalous or to represent changes in velocity with time as discussed below.

[16] The first line in Table 1 corresponds to 30 GPS points (upper C; green points in Figure 2) that were collected in the upper part of Ice Stream C [*Anandakrishnan et al.*, 1998]. Another 81 points (lower C, red) were collected on the lower part of Ice Stream C (H. Engelhardt, personal communication, 2000). Both these data sets were acquired using repeat GPS surveys and have small errors (e.g., <1 m/yr). In both cases, the GPS/SRI differences are similar in magnitude to the estimated differences from the error map.

[17] Velocity estimates were collected during the 1980s using Transit satellite receivers as part of the Siple Coast Project (SCP) [*Whillans et al.*, 1987; *Whillans and Van der Veen*, 1993]. The SCP/SRI differences are a little more than

Table 1. Comparison of Velocity Differences From Field Measurements With Estimated Errors (Figure 2)

Location	Number of points	σ_x (m/yr)	σ_y (m/yr)	Estimated σ_{v_x} (m/yr)	Estimated σ_{v_y} (m/yr)
Upper C (green)	30	1.1	0.8	1.7	0.4
Lower C (red)	81	1.3	1.2	1.4	0.9
SCP (blue)	63	4.2	4.0	1.9	1.8
D Onset grid (yellow)	223	2.5	4.0	0.8	1.3

Standard deviations of the differences between SRI and field measurements of velocity are denoted σ_x and σ_y. Errors in the field measurements in general are small, so the differences are representative of the SRI errors. Magnitudes of corresponding sample mean errors are all less than 1.4 m/yr. Estimated errors are tabulated as standard deviations (σ_{v_x}, σ_{v_y}). Colors in the first column refer to the symbols used to plot field measurement locations in Figure 2.

twice as large as the corresponding estimates of SRI error. Part of this difference may be due to the larger errors in SCP Transit data. While errors of 0.4 m/yr are cited for the SCP data [*Whillans and Van der Veen*, 1993], larger errors are acknowledged for some of the points with less tracking data. Some of the difference might also be attributable to changes in the velocity over the roughly 12 years between collection of the SCP and SRI data. While the 15 m/yr threshold we used was designed to eliminate points with significant temporal change, we are unable to discriminate smaller temporal differences from noise. Finally, some of the SCP points may fall in regions where the SRI data have locally large streak errors where our error estimates are biased low.

[18] For the field measurements at the onset of Ice Stream D [*Chen et al.*, 1998], the GPS/SRI differences are somewhat larger than the estimated SRI errors. Note that in evaluating these differences, we used a version of the velocity map that did not include the regridded onset points. Both the SRI and GPS data were collected at approximately the same time, so it is unlikely that the differences are due to temporal velocity change. The GPS errors (<1 m/yr) are too small to explain the difference. Close inspection of the data suggests that the onset grid lies in an area of locally strong streaks that have sufficient magnitude to explain the large differences.

[19] Overall, the data in Table 1 indicate that we obtained reliable estimates of the error at most locations, but there remain some areas where locally large streak errors cause us to underestimate the error. We do not have a reliable means to estimate the spatial distribution of streak errors, so the variability of this error is not included in our error estimates. With the exception of areas with strong streaks, comparison with the several hundred in situ measurements indicates that each component of our velocity estimate has errors ranging from about 1 to 4 m/yr.

3. Deceleration on Ice Stream A and Whillans Ice Stream

[20] Earlier studies have indicated deceleration on Whillans Ice Stream as summarized by *Whillans et al.* [2001]. These studies have generally been limited to areas where there were repeat surveys spaced several years apart. Here we are able to compare our data from 1997 with the several hundred field-based measurements of velocity that have been made over the last three decades. We first partitioned the in situ measurements into two groups: points with differences less than 15 m/yr and points with differences greater than 15 m/yr. The differences in the former group may be due to errors as described above. The velocity differences for the latter group likely reflect change in flow velocity with time and are plotted in Figure 3 along with their original station designations [*Whillans and Van der Veen*, 1993; *Thomas et al.*, 1984]. The majority of the differences correspond to SCP measurements made from 1984 to 1991 [*Whillans et al.*, 1987; *Whillans and Van der Veen*, 1993; *Price and Whillans*, 1998; *Stephenson and Bindschadler*, 1988]. Figure 3 also shows differences for eight velocity measurements from the Ross Ice Shelf Geophysical and Glaciological Survey (RIGGS), which were acquired from 1972 to 1974 [*Thomas et al.*, 1984]. Because of the large velocity differences, none of the points shown in Figure 3 were used as control points for interferometric baseline estimates. We note that we are comparing velocities at absolute geographic coordinates, not at old camps or survey poles on and moving with the ice through gradients in velocity.

[21] Velocity differences at SCP stations 91, 101, 107, 137, and 144 seem anomalously large and do not always coincide with the direction that would be expected for an along-flow change in speed. Measurements at these five stations each include a position measurement made in late December 1991 and none of these points were published by *Whillans and Van der Veen* [1993]. We believe that these five SCP measurements have large errors and that the velocity differences are not the result of changes in flow speed. Two velocity differences on Crary Ice Rise (E2.1 and E3) are larger than expected. *Whillans and Van der Veen* [1993] note, however, that these two measurements were made using less precise orbits and tracking data of poorer quality. Station 58 lies near a shear margin, so the apparent increase in velocity could result from the limited resolution (0.5–3 km) of the SRI data. The difference at station W3 suggests an inward migration of shear margin on the ice plain of Whillans Ice Stream. Although there were adequate tracking data, this measurement was made using less precise orbits [*Whillans and Van der Veen*, 1993], making it difficult to determine whether the velocity difference represents change or measurement error. The majority of remaining points were made using the more precise orbits and tracking data. With the exception of the outliers just described, other SCP measurements that were derived using orbits or tracking data of lesser quality [*Whillans and Van der Veen*, 1993] were consistent with neighboring points using the higher quality data.

[22] The remaining points shown in Figure 3 indicate a widespread pattern of deceleration on Whillans Ice Stream. Table 2 summarizes the velocity differences for several groups of nearby measurements. The average slowdown for six stations (Table 2) on the ice plain of Whillans Ice Stream is 71 m/yr over a roughly 12 year interval, which yields an average deceleration rate of 5.7 m/yr^2. RIGGS points collected over an interval roughly twice as long (1974–1997) yield similar deceleration rates on the ice plain of 5.0 and 5.6 m/yr^2 at stations F7 and G8, respectively. *Stephenson and Bindschadler* [1988] estimated similar deceleration rates for the interval separating the collection of the SCP and RIGGS data. Thus, the ice plain appears to have undergone a sustained and fairly steady deceleration over at least the period from 1974 to 1997.

[23] *Bindschadler and Vornberger* [1998] determined displacements of features in a pair of images spanning the interval from 1963 to 1989 and estimated an average deceleration of 19 m/yr^2, which is considerably larger than our estimates from 1974 to 1997. This means that deceleration rates of 40–60 m/yr^2 during the period from 1963 to 1974 are needed to make their estimates consistent with our observations over the interval from 1975 to 1997. There appears, however, to have been some distortion in the AVHRR imagery used to make their estimate (T. Scambos, personal communication, 2000). As a result, we performed two independent coregistrations of the original 1963 Corona image with the RADARSAT Antarctic Mapping Project

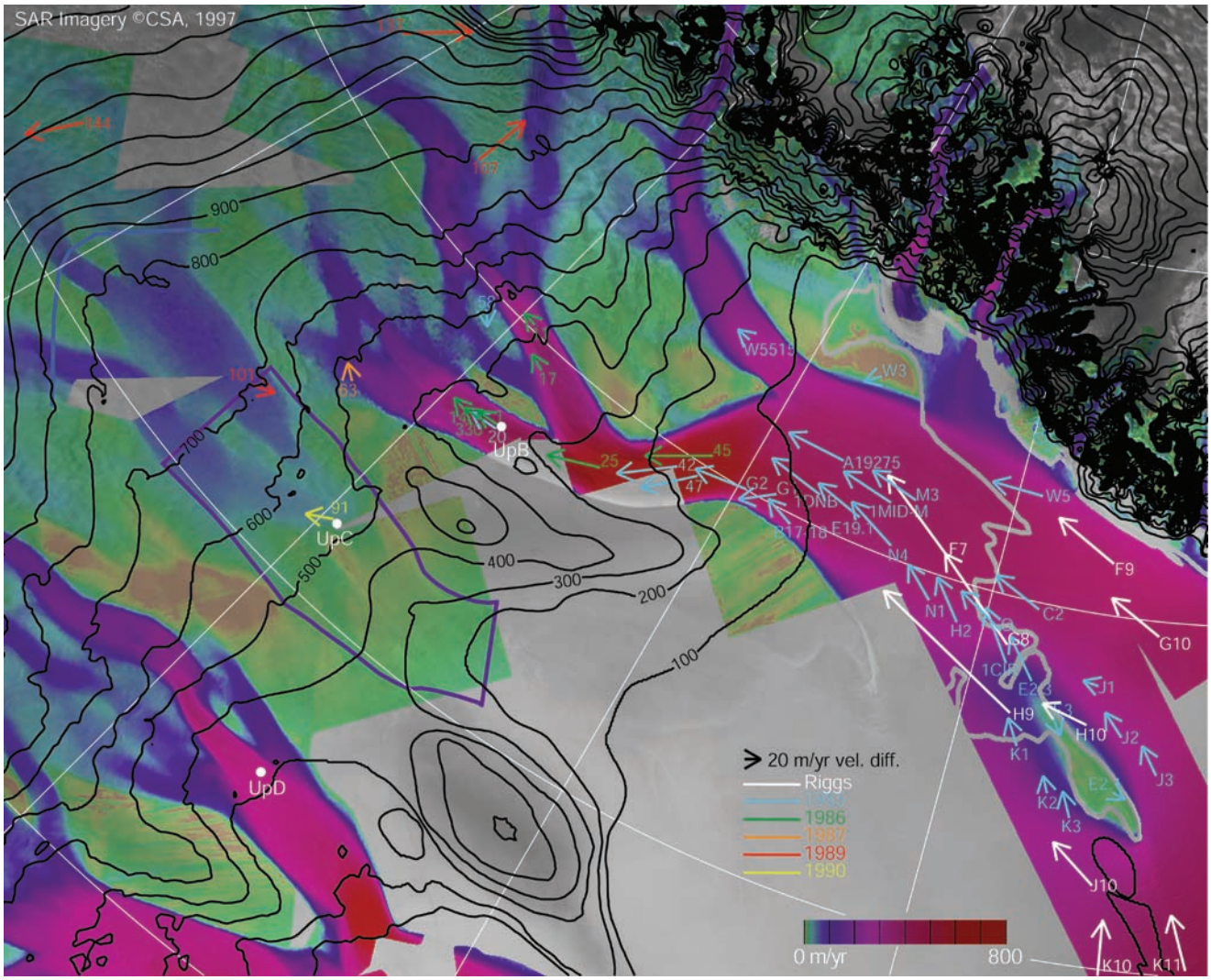

Figure 3. Differences between field measurements of velocity and SRI velocities (vectors). Vectors are color coded by the year (average of two survey dates) the field measurements were acquired. Text adjacent to each vector provides the station name [*Whillans and Van der Veen*, 1993]. The blue line and purpleout line are discussed in the text.

(RAMP) SAR mosaic to obtain estimates of 15 and 17 km for the displacement of "ice raft A" over the period from 1963 to 1997, which yields an average velocity of 441–500 m/yr. Assuming a linear deceleration and using the 1997 value of 406 m/yr, this yields estimates in the range from 474 to 594 m/yr for the 1963 velocity. The corresponding rate of deceleration ranges from 2.0 to 5.5 m/yr^2, which is in much closer agreement with the rates given in Table 2 than the original estimate [*Bindschadler and Vornberger*, 1998].

[24] The average deceleration rate for three points (42, 45, 47) within "the Narrows" (the portion of the ice stream between 100 and 300 m elevation) is 6.5 m/yr^2. Farther

Table 2. Average Values, Differences, and Deceleration Rates for Groups of SCP and RIGGS Stations Shown in Figure 3

Stations	Mean SRI speed (m/yr)	Mean transit speed (m/yr)	Mean magnitude of velocity difference (m/yr)	Mean rate of deceleration (m/yr^2)
A19275, 1DNB, 1MID-M, E19.1, M3, N4	404	474	71	5.7
42, 45, 47	693	769	77	6.5
1, 14, 20, 330	412	440	29	2.6
11, 17	349	370	21	1.9
F7	411	530	122	5.0
G8	249	384	137	5.6
H9	147	348	218	9.0
J10,K10,K11	381	450	71	3.0

Deceleration rates are determined by dividing the velocity differences by the time intervals separating measurements.

upstream on Whillans Branch 2 (B2), four points in the area around the UpB camp [*Whillans and Van der Veen*, 1993] indicate an average slow-down of 29 m/yr and a corresponding deceleration rate of 2.6 m/yr^2. This agrees well with measurements made by *Echelmeyer and Harrison* [1999], which show a change in velocity at UpB from 1984/1985 to 1994/1995 of 22 m/yr. A comparable decrease in velocity was also observed at UpB by *Hulbe and Whillans* [1997] from 1984/1985 to 1991/1992. On the upper part of Whillans Branch 1 (B1), two SCP/SRI differences yield a deceleration rate of 1.9 m/yr^2. A single point on Ice Stream A suggests a slowdown of similar magnitude.

[25] Figure 3 shows several velocity differences on the Ross Ice Shelf. The SCP/SRI velocity differences range from 20 to 68 m/yr, while the RIGGS/SRI velocity differences range from 61 to 88 m/yr on the ice shelf. The RIGGS/SRI differences averaged over three stations (J10,K10,K11) indicate that there is significant deceleration (Table 2) on the ice shelf even at distances of 50–100 km downstream of Crary Ice Rise.

[26] Estimates of the errors for the SCP points range from 0.4 m/yr [*Whillans and Van der Veen*, 1993] to 8 m/yr [*Stephenson and Bindschadler*, 1988]. The average SRI error estimate for the points shown in Figure 3 is just under 3 m/yr, so the 1-sigma errors for the SCP/SRI velocity differences range from 3 to 8 m/yr. All the differences in Figure 3 are larger than 15 m/yr and in many cases are almost an order of magnitude larger than the 1-sigma errors. *Thomas et al.* [1984] give what they term a conservative estimate of 15 m/yr for the velocity error. The smallest velocity difference for the RIGGS points shown in Figure 3 is 60 m/yr at H10, which is 4 times the error of 15 m/yr. Thus, errors in the data account for, at most, a small fraction of the measured deceleration of Whillans Ice Stream.

[27] The results in this section confirm earlier localized estimates of deceleration on Whillans Ice Stream [*Stephenson and Bindschadler*, 1988; *Hulbe and Whillans*, 1997; *Bindschadler and Vornberger*, 1998; *Echelmeyer and Harrison*, 1999] and greatly expand the number of observations, revealing a pattern of slowdown that extends from Ice Stream A and the upper reaches of Whillans Ice Stream to well downstream of the grounding line.

4. Comparison of Velocity and Bed Topography

[28] While the data in Figure 1 provide a detailed picture of ice flow at the surface, this flow is largely influenced by controls at the bed. Here we compare our velocity data with the bed topography. The BEDMAP consortium has combined nearly all available ice thickness and bed elevation data sets to produce a Digital Elevation Model (DEM) of the bed and an ice thickness data set for all of Antarctica [*Lythe and Vaughan*, 2001]. These data are posted at 5 km intervals, although actual resolution depends on the density of the source data. Fortunately, extensive radio echo mapping efforts [*Retzlaff et al.*, 1993; *Blankenship et al.*, 2001] have made the area shown in Figure 1 one of the better-mapped areas in Antarctica. Figure 4 shows a shaded surface rendering of the BEDMAP topography for the area shown in Figure 1. The artificial light source is directed roughly from the south and was selected to highlight subglacial valleys and troughs aligned with the general direction of flow, which generally trends from east to west. Bed elevation contours are plotted in black. Flow speed is color coded and displayed over the bed topography to illustrate the correspondence between bed topography and ice flow, which is discussed in more detail in later sections.

5. Force Balance

[29] In this section we apply the force-budget technique to examine the large-scale balance of forces on the ice streams and their tributaries. Ice flow is driven by gravity (driving stress) and is resisted by basal and lateral drag and gradients in the longitudinal stress [*Whillans*, 1987]. The partitioning of these resistive stresses can be estimated using the force-budget technique [*Whillans*, 1987; *Van der Veen*, 1999], which estimates stresses using observed strain rates.

5.1. Theoretical Background

[30] *Whillans and Van der Veen* [1993] have shown that on Whillans Ice Stream longitudinal stress gradients are relatively insignificant over length scales greater than several ice thickness. Their application of the force-budget technique to three areas on Whillans Ice Stream indicated that lateral drag is the primary restraint on flow [*Whillans and Van der Veen*, 1997]. With the data shown in Figure 1, we are able to apply the force-budget technique to many other locations to determine the relative roles of lateral and basal drag.

[31] We used a methodology based on that of *Whillans and Van der Veen* [1997]. We began by computing the strain rates for the entire velocity field. To reduce noise, the velocity data were smoothed with a moving average filter of width 3.5 km. At each point, we computed the strain rates using a local coordinate system with the *x axis* aligned with the direction of flow. Lateral shear stress, R_{xy}, was calculated as [*Van der Veen*, 1999]

$$R_{xy} = B\dot{\varepsilon}_e^{\left(\frac{1}{n}-1\right)}\dot{\varepsilon}_{xy}, \tag{1}$$

where n and B are the Glen's flow-law parameters, $\dot{\varepsilon}_{xy}$ is the horizontal shear strain rate, and $\varepsilon_e = \sqrt{0.5\left(\varepsilon_{xx}^2 + \varepsilon_{yy}^2 + \varepsilon_{zz}^2\right) + \left(\varepsilon_{xy}^2 + \varepsilon_{xz}^2 + \varepsilon_{yz}^2\right)}$ is the effective strain rate.

[32] The flow-law parameter, B, used to relate stress and strain in equation (1) is temperature dependent. We estimated this temperature dependence using an analytical solution to the steady state vertical thermal diffusion and advection equation [*Zotikov*, 1986, equation (4.17)]:

$$T = T_{pmp} - \left(T_s - T_{pmp}\right)\frac{erf\left(\sqrt{0.5Pe}\,\frac{z}{H}\right)}{erf\left(\sqrt{0.5Pe}\right)}, \tag{2}$$

where T_{pmp} is the pressure melting point, T_S is the surface temperature, H is ice thickness, and z denotes the vertical coordinate (zero at the bed and H at the top). The Peclet number is defined as $Pe = \frac{ah}{\kappa}$, where a is the surface accumulation rate and κ is the thermal diffusivity of ice.

[33] We used gridded accumulation and surface temperature data sets [*Giovinetto et al.*, 1990; *Giovinetto and Bentley*, 1985] for the estimates of T_S and a needed in equation (2). The ice thickness values, H, were determined from BEDMAP data and are tabulated in Tables 3 and 4. The theoretical temperature profiles were used to estimate depth-averaged values of B (Tables 3 and 4) through

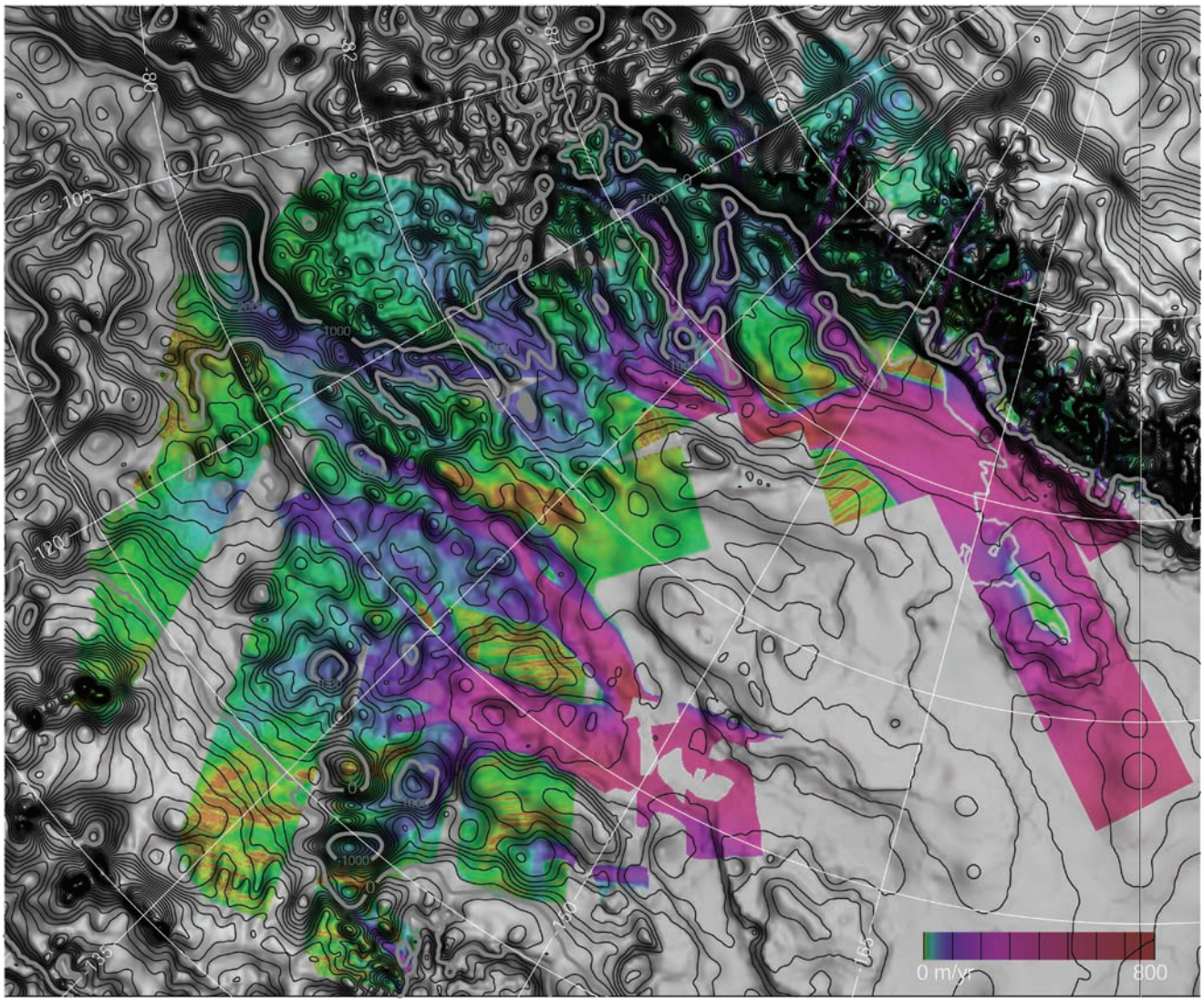

Figure 4. Ice stream speed (color) plotted over shaded surface rendering of the BEDMAP data. Bed elevations are also contoured at 100 m intervals (black), with gray used for 1000 m contour intervals.

numerical integration of the Arrhenius relationship [e.g., *Jackson and Kamb*, 1997, equation (18)]. For our study areas, the lowermost value of 530 kPa $yr^{1/3}$ was obtained for the ice plain of Whillans Ice Stream, while B exceeded 600 kPa $yr^{1/3}$ on several tributaries.

[34] Despite the fact that the ice streams may not be in a steady state, the existing temperature measurements from the study area can be approximated reasonably well using this equation. At the UpB [*Engelhardt and Kamb*, 1993], UpC, and UpD (Engelhardt and Kamb, personal communication, 2001) camps, values of B determined from measured profiles are 552, 651, and 627 kPa $yr^{1/3}$, respectively. The UpB value is close to the theoretical value for Whillans Ice Stream (Tables 3 and 4). The UpC and UpD values, however, suggest that our estimates of B in Tables 3 and 4 may be biased low by roughly 10–20% for Ice Streams C

Table 3. Driving Stress, Lateral Drag, Slope, and Thickness for Ice Streams at the Locations Shown in Figure 5 (Dark Gray Boxes)

Location	$\bar{F}_{lat}$ (kPa)	τ_d (kPa)	τ_b (kPa)	Width (km)	Slope	Thickness (m)	B (kPa $yr^{1/3}$)
A	9.9 ± 0.3	14.9 ± 6.1	5.0 ± 6.1	39	−0.00136	1242	562
WB1	12.5 ± 0.4	12.5 ± 7.1	0.0 ± 7.1	35	−0.00117	1205	554
WB2	11.3 ± 1.1	10.8 ± 1.5	−0.5 ± 1.9	34	−0.00123	985	539
W Narrows	7.7 ± 0.5	7.6 ± 1.6	−0.1 ± 1.7	48	−0.00101	846	537
W plain	1.9 ± 0.2	3.0 ± 0.9	1.1 ± 0.9	121	−0.000463	735	530
C	5.4 ± 0.3	16.7 ± 1.8	11.3 ± 1.8	69	−0.00103	1805	603
D	5.3 ± 0.2	10.0 ± 0.8	4.7 ± 0.8	55	−0.00127	888	534
E	4.4 ± 0.5	15.3 ± 1.6	10.9 ± 1.7	78	−0.00187	916	545

Basal drag, τ_b, is determined using equation (4). Uncertainties represent one standard deviation. The widths, W, are computed as described in the text. The widths used in equation (3) are typically about 80–90% of the full width (see Figure 6).

Table 4. Driving Stress, Lateral Drag, Slope, and Thickness for Ice Stream Tributaries at the Locations Shown in Figure 5 (Light Gray Boxes)

Location	$\bar{F}_{lat}$ (kPa)	τ_d (kPa)	τ_b (kPa)	Width (km)	Slope	Thickness (m)	B (kPa yr$^{1/3}$)
TWB1	29.8 ± 2.8	47.5 ± 5.6	17.7 ± 6.3	25	−0.00244	2188	638
TWB2	20.2 ± 2.5	40.9 ± 3.1	20.7 ± 4.1	25	−0.00299	1538	605
TC1	25.2 ± 1.4	40.1 ± 8.7	14.9 ± 8.8	17	−0.00251	1802	616
TC2	10.6 ± 3.9	89.7 ± 5.2	79.1 ± 6.5	43	−0.004576	2196	630
TD1	24.0 ± 4.2	67.8 ± 3.2	43.8 ± 5.3	24	−0.00390	1952	634
TD2	14.2 ± 1.3	29.0 ± 1.8	14.8 ± 2.2	35	−0.00230	1412	586
TD3	13.4 ± 1.6	31.0 ± 4.2	17.6 ± 4.5	21	−0.00308	1126	560
TE	21.7 ± 2.5	44.9 ± 5.1	23.2 ± 5.7	19	−0.00428	1177	580

Basal drag, τ_b, is determined using equation (4). Uncertainties represent one standard deviation. The widths, W, are computed as described in the text. The widths used in equation (3) are typically about 80–90% of the full width (see Figure 7).

and D and their tributaries. The reason for the less accurate estimate of temperature for Ice Streams C and D may have to do with the origin of ice at depth (horizontal advection). Figure 1 indicates that the UpB area is fed from relatively slow moving ice drawn from not far upstream so that the temperature profile is strongly influenced by local accumulation and temperature. In contrast, UpD and UpC are fed by faster moving tributaries that originate near the ice divide where both surface temperature and accumulation favor lower temperatures at depth, leading to larger values of B.

[35] The average lateral drag, $\bar{F}_{lat}$, across an ice stream can be estimated as [*Whillans and Van der Veen*, 1997]

$$\bar{F}_{lat} = H\frac{R_{xy}\left(\frac{W}{2}\right) - R_{xy}\left(-\frac{W}{2}\right)}{W} \tag{3}$$

where W is the ice stream width. Neglecting longitudinal stress gradients, the width-averaged force balance for an ice stream can be expressed as

$$\tau_d = \tau_b + \bar{F}_{lat}, \tag{4}$$

where τ_d is the driving stress and τ_b is the basal shear stress. Unless otherwise noted, τ_d and τ_b are assumed to be width-averaged values. If $\bar{F}_{lat}$ is determined using equation (3) and τ_d is estimated from surface slope, then equation (4) can be solved to determine τ_b.

5.2. Sampling Method

[36] We used boxes to define sampling areas at the locations show in Figure 5. Each box was selected to sample an area with relatively uniform ice stream geometry. Within each box, we determined a series of profiles running across flow and spaced 1 km apart. Plots of velocity and R_{xy} along the profiles are shown for ice stream locations in Figure 6 and for tributary locations in Figure 7. The distance along each profile was normalized using the width, W, of the ice stream or tributary. Width was determined automatically for each profile by selecting the region with velocity greater than some threshold (typically 10 m/yr).

[37] The magnitude of R_{xy} in Figures 6 and 7 tends to peak just short of the margins. *Whillans and Van der Veen* [1997] observed a similar, although less pronounced, effect in their estimates. In our case, we believe that the roll-off near the margins is caused by the 3.5 km smoothing filter we used to reduce noise. This contention is supported by measurements of strain rate across the margin of Whillans B2 [*Echelmeyer et al.*, 1994]. These data show a jump in shear strain from 0.04 yr^{-1} (the peak value we estimate) to a peak of 0.07 yr^{-1} in a distance of less than 2 km. This peak in strain rate would be smoothed away by our filter. To diminish the impact of this effect, we determined $\bar{F}_{lat}$ using the minimum and maximum values for the lateral shear stress in equation (3) instead of the values at the margins. The distance between these extrema was used in place of W in equation (3). As a consequence, our estimates of lateral resistance only sample the central 80–90% of the ice stream width, as defined by our velocity criterion.

[38] Tables 3 and 4 give the force balance results for the locations shown in Figure 5. Each value is an average of the roughly 20–40 profiles in each box. We have included the standard deviation of these estimates as a measure of the uncertainty for the individual profiles. These values reflect errors in the underlying velocity data and the natural variability in the lateral drag over a box, but do not include systematic errors such as errors in the flow-law parameters. Although averaging over profiles should reduce the uncertainty, we use the standard deviations here as a conservative estimate for the error in the averaged result.

[39] Tables 3 and 4 also include estimates of driving stress, τ_d, determined using the RAMP DEM [*Liu et al.*, 2000] and the BEDMAP bed elevation data [*Lythe et al.*, 2001]. The quality of the source data for the RAMP DEM varies considerably [*Liu et al.*, 1999] with the best accuracy for the Siple Coast in regions where ERS altimeter [*Bamber and Bindschadler*, 1997] or dense airborne survey data [*Retzlaff et al.*, 1993] were available. Noisy elevation data cause slope errors that lead to errors in τ_d estimates. To mitigate against these errors and to characterize their effect, we estimated τ_d at 10 manually selected intervals roughly centered about each of the boxes shown in Figure 5. In most cases, the intervals were longer than the downstream dimension of the sampling box (>10 ice thickness), and we were careful to select a wide variation in sampling lengths. For each interval, we estimated τ_d along a number of parallel profiles and averaged the result. We then computed the standard deviation for the ten averaged results (Tables 3 and 4). In areas where the source data for the RAMP DEM were of good quality, the variability in the driving stress estimates was about 10–15%. On Ice Stream A and Whillans B1, where the elevation data are of poorer quality, the standard deviations of the τ_d estimates were roughly 50% of the mean values.

5.3. Ice Stream Force Balance Results

[40] On Ice Stream A we estimated a value of 9.9 kPa for the lateral drag. The uncertainty is large, so the estimates of

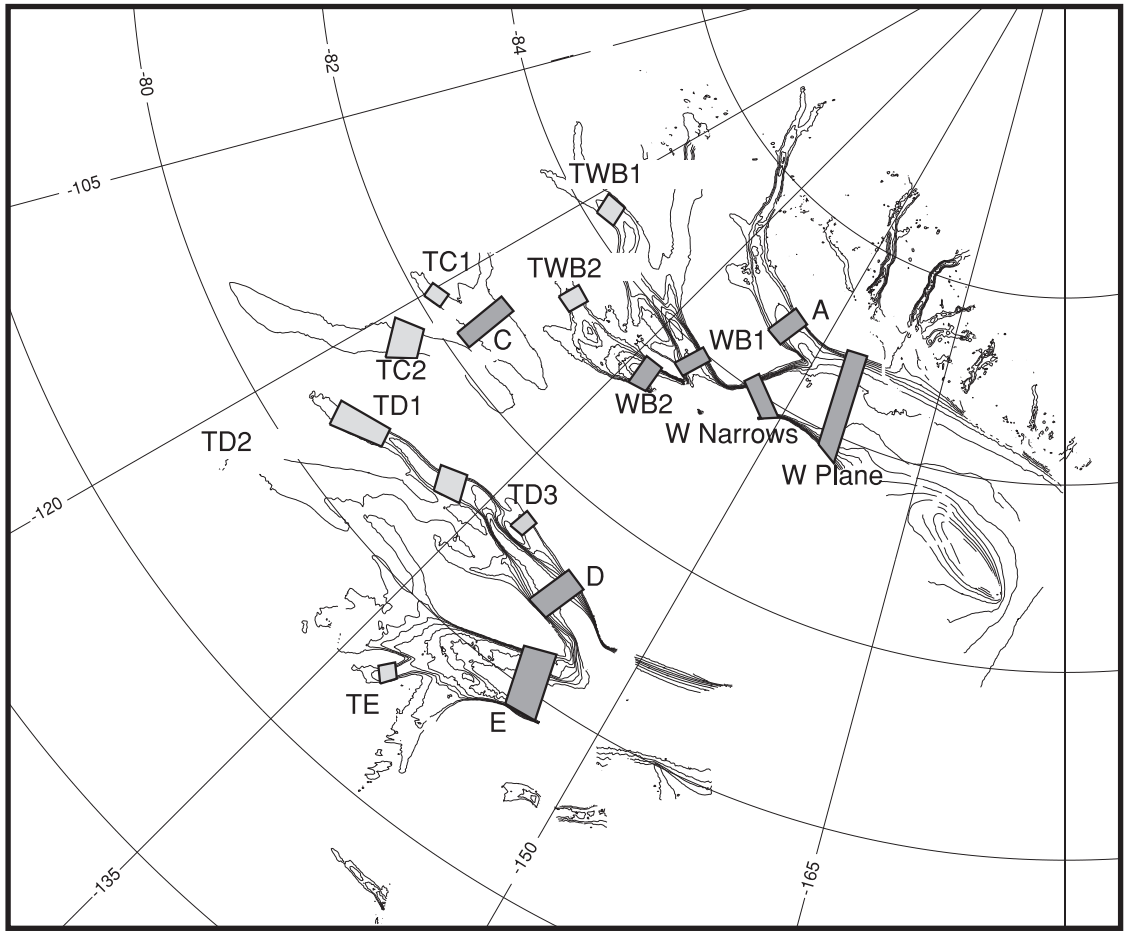

Figure 5. Locations of force balance calculations with dark gray boxes for ice streams and light gray boxes for tributaries. Contours at 50 m/yr are used to show ice stream/tributary locations.

τ_b range from between 0 and 53% of τ_d. The plots of R_{xy} show a nearly linear trend across the ice stream, which compares well with the linear dependence of R_{xy} expected for flow governed primarily by lateral drag. The velocity profiles indicate that Ice Stream A flows significantly slower than the other active ice streams.

[41] On Whillans B1, $\bar{F}_{lat}$ is just less than τ_d to yield an estimate of 0.0 kPa for τ_b. Here again the uncertainties are large, so that to within errors, τ_b ranges anywhere from 0 to 36% of the τ_d value. We note that our sampling region on Whillans B1 is farther downstream than the region sampled by *Whillans and Van der Veen* [1997]. We obtained values for $\bar{F}_{lat}$ and τ_d that are smaller than theirs by about 8 kPa, which likely reflects the widening of the ice stream between sampling locations. On Whillans B2, our sampling region roughly coincides with that of *Whillans and Van der Veen* [1997]. Our estimate of $\bar{F}_{lat}$ = 11.3 kPa agrees well with their estimate of 12–14 kPa. Although we obtained a nonphysical result of −0.5 kPa for τ_b, it is easily explained by the uncertainties in the data. The bed in this region supports 0–11% of the driving stress. The sampling box on the Narrows is slightly upstream of the "40 Block" examined by *Whillans and Van der Veen* [1997]. Our estimate of 7.7 kPa is comparable to their estimate of 7–10 kPa. The lateral drag is such that the bed supports only 0–17% of the driving stress.

[42] On the ice plain, $\bar{F}_{lat}$ = 1.9 kPa for τ_d = 3 kPa, so the bed supports 8–52% of the driving stress. Unlike the other Whillans Ice Stream profiles, the plots of R_{xy} do not exhibit an approximately linear trend. Instead, there is a roughly linear trend near the margins with a noisy but roughly level trend for the central part of the ice stream. This suggests that the effect of lateral drag is not transmitted into the central stream.

[43] The velocity profile for Ice Stream C indicates that while the ice stream is still moving, the speeds are nearly an order of magnitude less than on the other ice streams. There is no clear linear trend across the ice stream in the R_{xy} plot, so it is difficult to determine how the average lateral drag of 5.4 kPa is distributed across the ice stream. Neglecting longitudinal stress gradients, τ_b resists 67–74% of the driving stress. Longitudinal stress gradients may be a factor in this area, however, due to the along-flow deceleration as ice approaches the stagnant portion of the ice stream.

[44] The R_{xy} plots indicate a nearly linear trend across Ice Stream D, but with a considerable degree of variability near the central portion of the profiles. With a $\bar{F}_{lat}$ = 5.3 kPa, τ_b accounts for 42–51% of τ_d.

[45] The plots of R_{xy} across Ice Stream E show a high degree of variability with a corresponding degree of variability visible in the velocity profiles. Lateral drag only supports an average of 4.4 kPa, while basal drag accounts for 64–71% of the resistance to the driving stress.

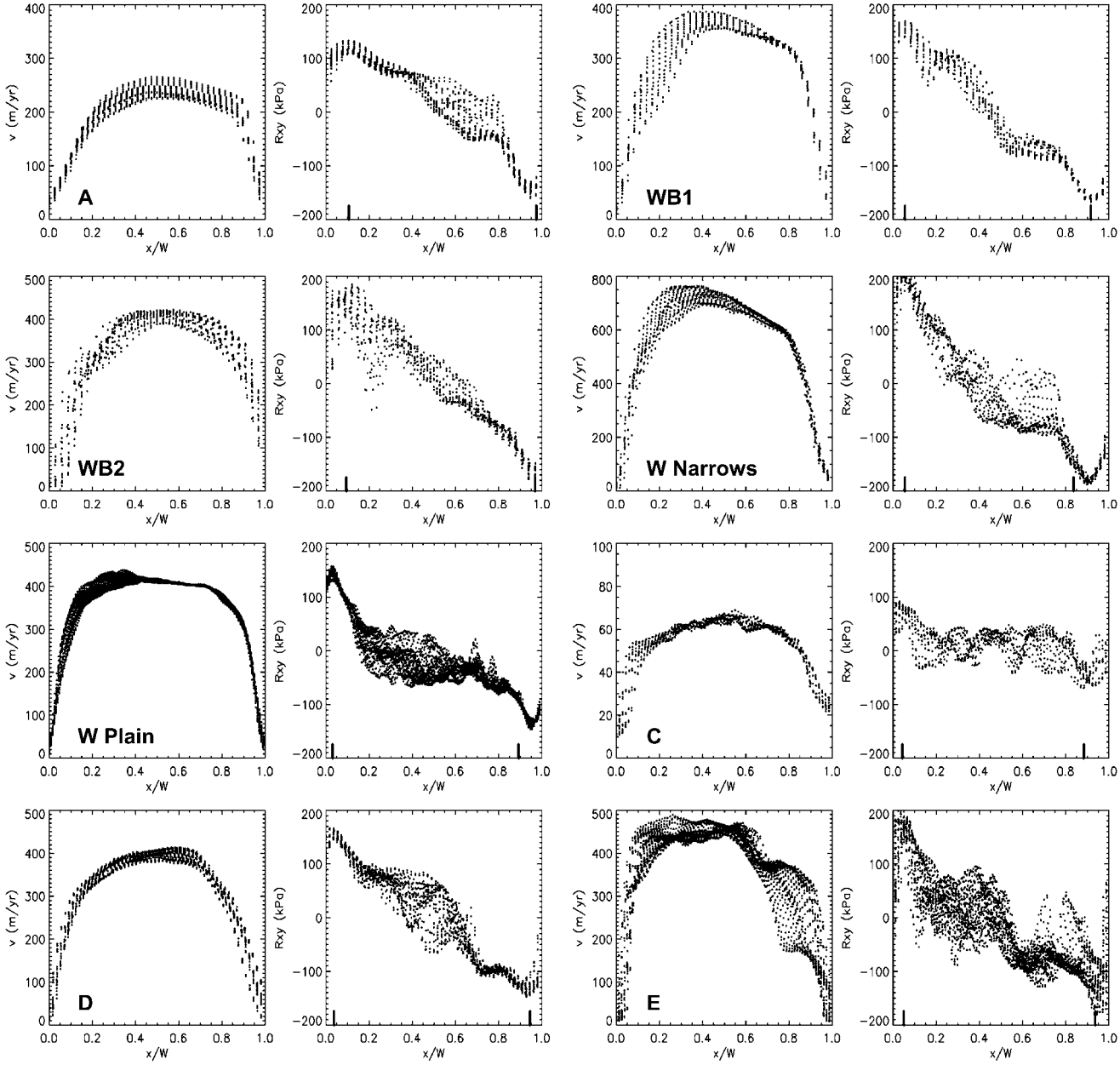

Figure 6. Velocity and R_{xy} plots for several ice stream locations (see Figure 5). The thick vertical lines along the *x axis* of the R_{xy} plots indicate average locations of the R_{xy} used for determining lateral drag.

[46] The force balance estimates depend strongly on the parameters used in the flow law. Analysis based on modeling constrained by measurements across the margin of Whillans B2 near the UpB camp initially indicated that strain softening and viscous heating could lead to strain rate enhancement factors of 10–12.5 [*Echelmeyer et al.*, 1994]. Enhancement factors this large would considerably decrease our estimates of lateral drag. Subsequent analysis by the same authors of the internal heat production based on model fits to temperature data, however, suggested a lateral shear stress of 200 kPa and a lateral resistance of 12 kPa [*Harrison et al.*, 1998]. Laboratory tests of ice samples extracted from the margin near UpB indicate a lateral shear stress of 220 kPa [*Jackson and Kamb*, 1997]. The latter two results, which make no assumptions about the flow-law parameters, suggest little or no enhancement. Both results are consistent with our estimates for Whillans B2. Given that other ice streams should experience similar thermal and strain histories at the margins, we conclude that relatively little error is introduced in our results by our neglecting to include strain rate enhancement in the flow law.

5.4. Tributary Force Balance Results

[47] While the ice streams themselves have been the subject of intensive study, little work has been done on the tributaries that feed them. *Hulbe et al.* [2000] concluded that deformation flow could account for a significant fraction of the motion. In this section, we use the force balance technique to evaluate the role of lateral drag at the locations shown in Figure 5 (light gray boxes). Plots of tributary velocity and lateral shear stress are shown in Figure 7 with force balance estimates summarized in Table 4.

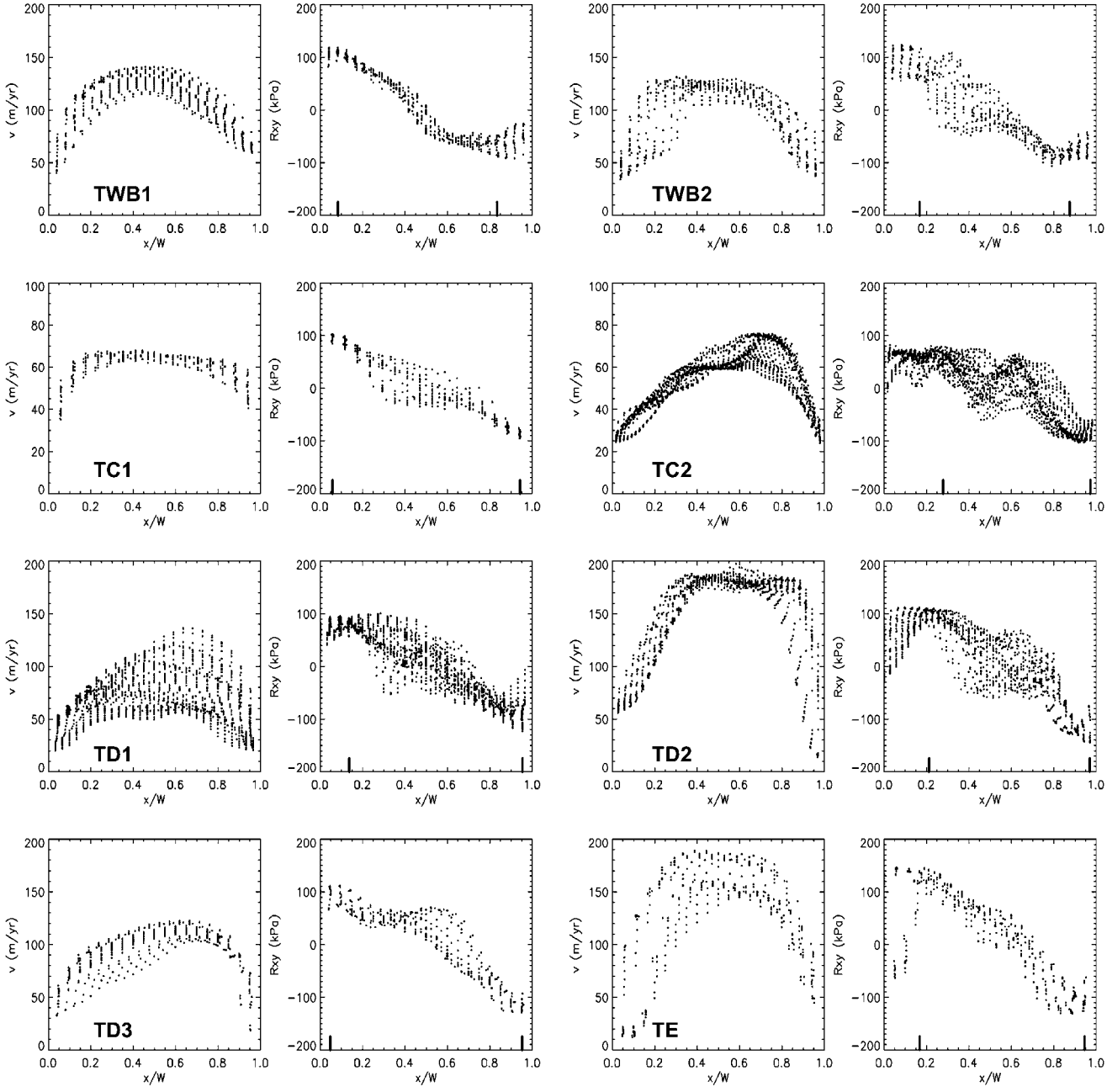

Figure 7. Velocity and R_{xy} plots for several tributary locations (see Figure 5). The thick vertical lines along the *x axis* of the R_{xy} plots indicate average locations of the R_{xy} used for determining lateral drag.

[48] With speeds of roughly 150 m/yr, the tributaries of Whillans B1 and B2 move considerably slower than do their respective ice streams. The shear margins are less well pronounced, and the ice adjacent to the tributaries moves at greater speeds (10–20 m/yr) than ice just outside the ice stream margins (1–5 m/yr). At roughly 100 kPa, lateral shear stresses are about half that observed at the ice stream margins. With narrower widths and thicker ice, however, $\bar{F}_{lat}$ values of 29.8 kPa at TWB1 and 20.2 at TWB2 are significantly greater than values found on the ice streams. Basal drag takes up 27–45% of the driving stress at TWB1 and 44–56% driving stress at TWB2.

[49] With a lateral drag of 25.2 kPa, τ_b supports 19–49% of the driving stress at TC1. The large tributary of Ice Stream C that follows the Bentley Subglacial Trough is sampled with the box at TC2. The lateral drag is only 10.6 kPa for this tributary and basal drag supports 86–90% of the driving stress, which is a much larger fraction than for the other tributaries.

[50] We sampled the long tributary of Ice Stream D at two locations along its length (TD1 and TD2, Figure 5). At the location furthest inland, TD1, τ_d is the greatest at 67.8 kPa. Lateral drag was 24.0 kPa so that basal resistance supports 60–69% of the driving stress. Farther downstream at TD2, the lateral drag dropped to 14.2 kPa for a τ_d value of 29.0 kPa so that basal drag resists 46–55% of the driving stress. At location TD3 we sampled the slower branch where the tributary divides to flow around a nearly stationary "island"

just above the ice stream. Here we obtained a lateral drag of 13.4 kPa for a driving stress of 44.9 kPa.

[51] On Ice Stream E we sampled a small tributary at TE with similar geometry to the tributary at TC. Here we obtained similar values to TC with a driving stress of 44.9 kPa opposed by a lateral drag of 21.7 kPa and a basal drag of 23.2 kPa.

6. Analysis

6.1. Flow in Ice Stream Tributaries

[52] The velocity map in Figure 1 as well as earlier velocity [*Joughin et al.*, 1999] and image [*Hodge and Doppelhammer*, 1996] maps reveal that the Siple Coast ice streams are fed by a system of tributaries, many of which branch to feed more than one ice stream. Here we examine various aspects of tributary flow and how it differs from ice stream flow.

[53] Figure 4 reveals that the tributaries tend to follow subglacial valleys as indicated in an earlier less extensive comparison [*Joughin et al.*, 1999]. Analyses of aerogeophysical and seismic data have indicated that a tributary of Ice Stream C (TC in Figure 5) coincides with a fault-bounded sedimentary basin with sediment infill in the range of 1.4–2 km [*Bell et al.*, 1998; *Anandakrishnan et al.*, 1998]. Additional aerogeophysical gravity, magnetic, and radar-echo sounding data in the catchments of Whillans Ice Stream B and Ice Stream C have also revealed sedimentary basins [*Blankenship et al.*, 2001] that coincide well with tributary flow [*Studinger et al.*, 2001]. The strong coincidence of tributaries with subglacial valleys (Figure 4) suggests that the rest of the tributary system may also lie on top of a relatively thick (e.g., >100 m) layer of consolidated sediment.

[54] *Hulbe et al.* [2000] found that a significant fraction of the tributary motion could be explained by ice deformation (vertical shear). The model used in that study, however, does not account for lateral drag. If lateral drag supports roughly half the driving stress as the data in Table 4 indicate, then estimates of vertical shear within the ice column are much smaller (reduced by a factor of ~8). In the absence of significant vertical shear, tributary flow is dominated by basal motion. An exception may be the large tributary that coincides with the Bentley subglacial trough, which has a large driving stress, most of which is supported by the bed.

[55] The rapid motion of ice streams has been attributed to a several meter thick layer of water-saturated dilatant till beneath the ice streams [*Blankenship et al.*, 1987]. Debate remains over whether the fast motion is enabled by deforming till [*Alley et al.*, 1987; *Kamb*, 2001] or by sliding at the ice–till interface due to a weak plastic bed [*Kamb*, 1991; *Tulaczyk et al.*, 2000a, 2000b]. Seismic analysis of data from one of the tributaries of Ice Stream C (near TC1 in Figure 5) suggests a layer of dilatant till at least 2 m thick (S. Anandakrishnan, personal communication, 2001). Other than this result, it has not been determined whether or to what extent a similar dilatant till layers exists beneath the tributaries. Regardless of the till mechanics, the force balance estimates (Table 4) indicate that beds beneath the tributaries support basal shear stresses of ~20 kPa, which is roughly an order of magnitude greater than τ_b beneath much of the ice streams (~2 kPa). This suggests that the processes giving rise to rapid basal motion beneath the tributaries differ significantly from those beneath the ice streams.

[56] In any hypothesis involving basal sliding or deforming till, water is an essential ingredient for lubrication. Basal melt rate, m_r, is determined by [*Paterson*, 1994]

$$m_r = \frac{G + \tau_b U_b - k_i \Theta_b}{L_i \rho_{ice}}, \tag{5}$$

where G is the geothermal heat flux, $\tau_b U_b$ is the basal shear heating given the basal speed U_b, k_i is the thermal conductivity for ice, Θ_b is the basal temperature gradient, L_i is the latent heat of fusion, and ρ_{ice} is the density of ice. A typical tributary with a speed of U_b = 100 m/yr and τ_b = 20 kPa, yields a melt rate of 5.2 mm/yr for G = 70 mW/m^2 and Θ_b = 0.04°C/m. This contrasts with a melt rate of 1.2 mm/yr for an ice stream with the same G and Θ_b moving at 400 m/yr over a bed with τ_b = 2 kPa. Furthermore, thicker ice in the tributaries should also lead to smaller basal temperature gradients and further enhance basal melt relative to the ice streams.

[57] Both the viscous-deforming bed [*Alley et al.*, 1987; *Blankenship et al.*, 1987] and the plastic bed models [*Kamb*, 1991; *Tulaczyk et al.*, 2000a, 2000b] transport till downstream, although till fluxes differ by roughly one order of magnitude [*Tulaczyk et al.*, 2001]. In either case, a source is needed to replenish till carried away by ice streamflow. Well lubricated ice streams with only a few kPa of basal resistance are unlikely to yield significant erosion of the consolidated sediments beneath the several meter thick dilatant till layer [*Cuffey and Alley*, 1996]. Inland ice frozen to the bed should also yield little erosion. *Bell et al.* [1998] suggested that scouring of the bed in the sedimentary basin they studied may provide a source of till to enable rapid motion downstream. This notion is consistent with the stronger basal shear indicated by the force balance estimates (Table 4). A stronger bed suggests a much thinner or patchy layer of lubricating till that allows greater contact of the ice with the consolidated sediments, yielding erosion that supplies the ice streams with lubricating till. Thus, tributaries may act as the prime source of lubricating till needed to sustain ice stream motion.

[58] In general, tributaries appear to be characterized by driving stresses in the range of about 30–90 kPa, beds that support roughly half this driving stress, a strong correspondence with subglacial valleys, and relatively narrow widths (15–45 km). This is in contrast to ice streams, which generally have lower driving stresses, weaker beds, greater widths, and do not lie in distinct basal troughs. We note that the distinction between ice streams and tributaries may be somewhat artificial. In an absolute sense, both involve relatively weak beds and lateral resistance takes up a significant fraction of the driving stress. In a relative sense, though, the bed resistance beneath much of the ice streams is nearly an order of magnitude smaller than for the tributaries. While this might only reflect the amount and spatial distribution of lubricating till, we feel that until more is known it is important to make a distinction between tributary and ice stream flow.

6.2. Onset of Tributary and Streaming Flow

[59] The "ice stream onset" or simply "onset" has been defined as the location of the transition from inland to

streaming flow [*Bindschadler et al.*, 2001]. Inland flow is taken to mean sheet flow with ice that is frozen to the bed. Streaming flow has been defined as rapid motion despite low driving stresses. The concepts of an ice stream onset predates the discovery of the network of tributaries that provide an extended transition from inland ice to ice streamflow and complicate the notion of an onset.

[60] One of the more common definitions for an onset is the location where speed increases rapidly along-flow despite a drop in the driving stress. A more restrictive definition based on driving stress [*Whillans et al.*, 2001] is that upstream of the onset speeds are less than 300 m/yr, the driving stress ranges from 20 to 70 kPa, and basal drag is the dominant restraint. Downstream of the onset, τ_d is less than 10 kPa, the resistance is primarily from lateral drag, and the speeds are greater than 300 m/yr. By this definition, the tributaries visible in Figure 1 lie upstream of the onset. *Blankenship et al.* [2001] define an onset as the region where the transition to rapid basal motion takes place. By this definition, tributaries are located downstream of the onset since they move largely by basal motion. In this case, the onset may be separated from its respective ice stream by several hundred kilometers. If we make a distinction between ice streams and tributaries as described above, then much of the ambiguity in onset definition is removed by also making a distinction between ice stream and tributary onsets.

[61] The onsets of ice streamflow are visible in Figure 1 as the locations where speed increases rapidly from the tributaries ($\sim$100 m/yr) to ice streams ($\sim$400 m/yr). Figure 4 indicates that at many of these locations, the rapid increase in speed occurs as ice emerges from the confining subglacial valleys of the tributaries to the flatter region with more subdued local topography that contains the ice streams. At these locations there is generally a doubling or more in width from tributary (W $\approx$ 20 km) to ice stream $W > 35$ km. Thus, ice stream onsets are often associated with a removal of lateral topographic constraints on width rather than a step in the subglacial topography as observed at other locations [*McIntyre*, 1985].

[62] Ice stream speed generally increases as W^4 [*Raymond*, 1996]. This means that the widening that takes place at the onset can account for some of the increase in speed and reduction in driving stress. For example, when bed resistance is held fixed, the transition from a 20 km wide tributary moving at 100 m/yr to a 40 km wide ice stream flowing at 400 m/yr is consistent with a roughly 10 kPa drop in τ_d (see equation (6)). In addition, the data in Tables 3 and 4 indicate that tributary beds provide significantly greater resistance ($\sim$20 kPa) than do ice streambeds ($\sim$2 kPa). Thus, ice stream onsets also appear to be governed by an along-flow transition to a weaker bed. Both of these factors likely contribute to the decrease in driving stress that is characteristic of ice stream onsets. As discussed above, basal melting is likely to be greater for tributaries than for ice streams in many instances, so the along-flow transition from tributary to ice stream is not coincident with the onset of basal melt (as occurs across lateral margins [*Raymond et al.*, 2001]).

[63] The onsets of tributary flow are visible in Figure 1 as the locations where inland ice flow increases abruptly to tributary speeds of roughly 50–150 m/yr (green-to-blue transitions). The tributaries are largely confined to a network of subglacial valleys, many of which have been observed to contain a deep layer of sediment infill [*Bell et al.*, 1998; *Anandakrishnan et al.*, 1998; *Blankenship et al.*, 2001; *Studinger et al.*, 2001]. Extrapolating these observations to the entire network of tributaries, the onset of tributary flow may be largely controlled by the transition to a bed with a thick layer of consolidated sediments and by the topographic constraints on width imposed by the bounding subglacial basins. These controls appear to constrain both the upstream limit and the lateral extent of tributary flow. In addition, the onset of tributary flow should coincide with the transition from a frozen to melted bed, with tributary speeds providing sufficient basal shear heating needed to sustain basal melting. The bounding subglacial basins may also play a role in this transition by providing the thicker ice needed to support melting.

[64] In this section we have expanded the notion of an onset to include both the ice stream and tributary onsets in a manner that is consistent with the ice stream/tributary distinction described above. As with any conceptual framework, it is always difficult to get perfect agreement between the idealization and reality. Whillans Ice Stream perhaps provides perhaps the best fit to the ideal with an order of magnitude or more difference in bed resistance from ice stream to tributary. The case for Ice Stream E is more murky, with the basal resistance for the ice stream only half that for its tributary, suggesting that the basal controls for this tributary and ice stream may not differ so greatly. Nevertheless, in following a flow line from the divide through a tributary and ice stream, there generally are two points along flow where a rapid increase in speed occurs, creating the need for some form of distinction.

6.3. Controls on Ice Stream Velocity

[65] In this section we examine the sensitivity to parameters determining ice stream speed using a simple model [*Raymond*, 1996], which gives the centerline speed, U, of an ice stream as

$$U = \frac{2AH}{(n+1)}(\tau_d - \tau_b)^n \left(\frac{W}{2H}\right)^4, \tag{6}$$

where A is the flow-law parameter [*Paterson*, 1994]. This equation can be substituted into equation (5) to provide the velocity dependence for the melt rate [*Tulaczyk et al.*, 2000b]. Using $\tau_d = \rho_{ice} g \alpha$ and letting $n = 3$, equation (6) can be rewritten as

$$U = \frac{A}{2}\left(\rho_{ice} g \alpha - \frac{\tau_b}{H}\right)^3 \left(\frac{W}{2}\right)^4, \tag{7}$$

where α denotes surface slope, and g is acceleration due to gravity. Differentiating this equation with respect to time yields

$$\begin{aligned}\dot{U} &= \frac{A}{2}\left[3\left(\rho_{ice} g \alpha - \frac{\tau_b}{H}\right)^2 \left(\rho_{ice} g \dot{\alpha} - \frac{\dot{\tau}_b}{H} + \frac{\tau_b}{H^2}\dot{H}\right)\left(\frac{W}{2}\right)^4 \right.\\ &\quad \left. + 4\left(\rho_{ice} g \alpha - \frac{\tau_b}{H}\right)^3 \left(\frac{W}{2}\right)^3 \left(\frac{\dot{W}}{2}\right)\right]\\ &= \frac{AH}{2}\left[3(\tau_d - \tau_b)^2 \left(H \rho_{ice} g \dot{\alpha} - \dot{\tau}_b + \frac{\tau_b}{H}\dot{H}\right)\left(\frac{W}{2H}\right)^4 \right.\\ &\quad \left. + 4(\tau_d - \tau_b)^3 \left(\frac{W}{2H}\right)^3 \left(\frac{\dot{W}}{2H}\right)\right].\end{aligned} \tag{8}$$

For small basal shear stress

$$(H\rho_{ice}g\dot{\alpha} - \dot{\tau}_b) \gg \frac{\tau_b}{H}\dot{H},$$

and if we assume

$$\dot{\tau}_d \approx H\rho_{ice}g\dot{\alpha},$$

then equation (8) can be approximated as

$$\dot{U} \approx \frac{AH}{2}\left[3(\tau_d - \tau_b)^2\left(\frac{W}{2H}\right)^4(\dot{\tau}_d - \dot{\tau}_b) + 4(\tau_d - \tau_b)^3\left(\frac{W}{2H}\right)^3\left(\frac{\dot{W}}{2H}\right)\right]. = \dot{U}_{\tau_d} + \dot{U}_{\tau_b} + \dot{U}_W. \quad (9)$$

This equation gives change in speed with respect to temporal change in geometry $\left(\dot{U}_{\tau_d},\ \dot{U}_W\right)$ and bed strength $\left(\dot{U}_{\tau_b}\right)$.

[66] Extensive laboratory and in situ testing of till strength beneath Whillans Ice Stream and ice streams C and D indicates that till behaves as a plastic material with yield strengths of only a few kPa and little dependence of strength on strain rate [*Tulaczyk et al.*, 2000b; *Kamb*, 1991, 2001]. With this model, dilatant till is strengthened when the void ratio, e, is decreased by removing water from the till, which can result from basal freezing or a change in drainage. An empirical relation for the dependence of bed strength is given as [*Tulaczyk et al.*, 2000b]

$$\tau_f = b_1\exp(-b_2 e) = 944,000\exp(-21.7e), \quad (10)$$

where τ_f is the failure strength of the plastic till. Equating τ_b to τ_f yields

$$\dot{U}_{\tau_b} = \frac{2AH}{(3+1)}\left[3(\tau_d - \tau_b)^2\left(\frac{W}{2H}\right)^4(21.7\tau_b\dot{e})\right] \quad (11)$$

From the work of *Tulaczyk et al.* [2000b], we get

$$\dot{e} = \frac{m_r - d_r}{Z_s}, \quad (12)$$

where d_r is the drainage rate and Z_s is the thickness of the dilatant till layer. Combining equations (11) and (12) yields

$$\dot{U}_{\tau_b} = \frac{AH}{2}\left[3(\tau_d - \tau_b)^2\left(\frac{W}{2H}\right)^4\left(\frac{21.7\tau_b(m_r - d_r)}{Z_s}\right)\right]. \quad (13)$$

If the width and thickness of an ice stream is held fixed, then equations (5), (6), and (13) provide a closed set of equations that describes the change in velocity as governed by the thermodynamic evolution at the bed. Equation (9) gives the sensitivity of flow speed to changes in thickness and width.

6.4. Application to Siple Coast Ice Streams

6.4.1. Whillans Ice Stream

[67] Figure 8a shows estimates of m_r, U, and $\dot{U}_{\tau_b}$ for the UpB camp computed using equations (5), (6), and (11), respectively. The three sets of curves correspond to τ_d values of 9.3, 10.8, and 12.3 kPa. This figure is modeled after a similar figure by *Tulaczyk et al.* [2000b], but with the addition of the $\dot{U}_{\tau_b}$ curves. The velocity curves calculated from equation (4) suggest that our estimate of $\tau_d = 10.8$ kPa is slightly low, as only the case where $\tau_d = 12.3$ kPa yields values that are consistent with observed speeds. Such an underestimate of τ_d is consistent with the finding of $\bar{F}_{lat} > \tau_d$ at UpB (Table 3), but also may be related to the simplified representation of the ice stream geometry. The melt rate curves (from equation (3)) depend on τ_b, but not on a specific till model [e.g., *Raymond*, 2000]. Melt rates are near zero for the estimated values of τ_b (0–1.1 kPa), suggesting little or no departure from undrained conditions.

[68] The $m_r = 0$ point at $\tau_b \approx 1.25$ kPa (Figure 8a) was determined to be a stable point [*Tulaczyk et al.*, 2000b] and

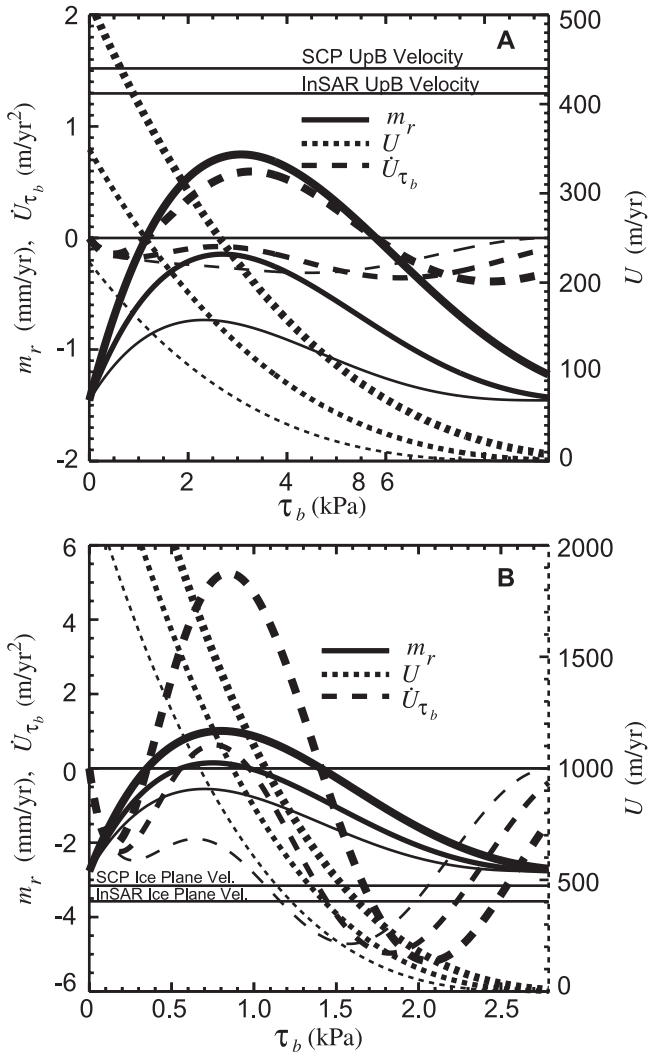

Figure 8. Modeled melt rate (m_r), centerline velocity (U), and bed strength velocity change $\left(\dot{U}_{\tau_b}\right)$ for (a) UpB parameters: $\Theta_b = 0.04$, $G = 70$ mW/m^2, $B = 540$ kPa yr$^{1/3}$, $W = 34$ km, $H = 985$ m, $Z_s = 6$ m, and $\tau_d = 12.3$ kPa (thick), 10.8 kPa (medium), and 9.3 kPa (thin), and (b) Ice plain parameters: $\Theta_b = 0.046$, $G = 70$ mW/m^2, $B = 540$ kPa yr$^{1/3}$, $W = 121$ km, $H = 735$ m, $Z_s = 6$ m, and $\tau_d = 3.2$ kPa (thick), 3.0 kPa (medium), and 2.8 kPa (thin).

lies in what *Raymond* [2000] calls the production-limited regime. About this point there is a negative feedback to change in velocity since an increase (decrease) in velocity is counteracted by a reduction (increase) in melting and lubrication. The plots in Figure 8a indicate that the ice stream operates in this stable regime at UpB. Unstable conditions exist about the $m_r = 0$ point near $\tau_b = 6$ kPa. Here the feedback is positive so that positive m_r causes an increase in velocity that leads to more melting and further velocity increases. If the melt rate goes negative, decreases in velocity increase freezing and the trend is continued toward complete shutdown.

[69] The $\dot{U}_{\tau_b}$ curves are computed using equation (13) under the assumption of an undrained plastic bed with a layer of dilatant till 6 m thick as has been measured seismically near the UpB and DownB camps [*Blankenship et al.*, 1987; *Rooney et al.*, 1987; *Alley et al.*, 1989]. For all values of τ_b, the magnitude of $\dot{U}_{\tau_b}$ at UpB does not exceed about 0.5 m/yr^2. As a result, for a fixed geometry with UpB parameters, the evolution of the bed strength due to velocity-induced changes in melt rate cannot explain the observed deceleration rate of 2.6 m/yr^2, even if the ice stream were operating in what is considered an unstable regime.

[70] We have assumed undrained conditions for the plastic bed model, which is consistent with the weak bed and near-zero melt rates. This simplifies theoretical developments since we have no experimentally verified theory describing either steady state or time-dependent behavior of the drainage rate, d_r, beneath ice streams and tributaries [*Engelhardt and Kamb*, 1997; *Kamb*, 2001]. Under reasonable assumptions regarding drainage (see discussion below), it is not possible to get the plastic bed model to transition to the unstable regime for conditions at UpB.

[71] The southern margin of Whillans B2 (Dragon) has been estimated to be widening at rates from 7 m/yr [*Harrison et al.*, 1998] to 17 m/yr [*Hamilton et al.*, 1998]. If such widening is symmetric, this would result in an increase in W of 14–34 m/yr. This yields values of $\dot{U}_W$ in the range from 0.7 to 1.6 m/yr^2 at the estimated widening rates and with $\tau_d - \tau_b = 11.4$ kPa, which is the value required to match the observed speed. As a result, the factors contributing to the slowdown are likely greater than indicated by the observed deceleration rates because they must also offset a trend toward acceleration due to widening.

[72] Changes in τ_d provide an effective way to modulate the velocity of an ice stream. Solving $\dot{U}_{\tau_d}$ for τ_d we find that $\dot{\tau}_d = -0.024$ kPa/yr matches the observed deceleration of 2.6 m/yr^2 with no widening, and a value of $\dot{\tau}_d = -0.039$ kPa/yr is required when widening at the maximum estimate of 34 m/yr is considered. Such change would be caused by a decrease in slope in the range from 2.7e−6 to 4.4e−6, which is equivalent to a thinning gradient of 0.27–0.44 m/yr over a distance of 100 km. Absolute thinning rates of 1 m/yr have been estimated for a region upstream of the UpB camp [*Joughin et al.*, 1999] and measured at 1.3 m/yr at UpB (G. Hamilton, personal communication, 2001). Although Whillans Ice Stream is nearly in balance at present [*Joughin and Tulaczyk*, 2002], faster speeds in the past (Figure 3) indicate that it recently had a negative mass balance. Thinning due to this imbalance might explain the observed deceleration in the vicinity of UpB. A similar analysis indicates that the Narrows section of Whillans Ice Stream is in the stable region of the plastic bed model and that a value of $\dot{\tau}_d = -0.022$ kPa/yr provides a good model fit to the observed deceleration rate.

6.4.2. Ice Plain of Whillans Ice Stream

[73] As a percentage of flow speed, the largest deceleration rates (~1.4%/yr) are observed on the ice plain of Whillans Ice Stream. Linear extrapolation of these rates yields zero velocity in 70–80 years. If a shutdown were to occur, the resulting cessation of the outflow from Ice Stream A and Whillans Ice Stream would result in a significantly greater positive regional mass balance for the Siple Coast ice streams than already exists due to the shutdown of Ice Stream C [*Joughin and Tulaczyk*, 2002]. Although caution needs to be exercised when extrapolating such results, we note that the deceleration appears to have been sustained at a relatively steady rate over an interval of at least two to three decades. Furthermore, the deceleration appears to continue well past Crary Ice Rise, indicating an interval long enough to allow the deceleration to propagate well downstream of the grounding line. This raises questions about the cause of the deceleration and whether it will continue all the way to a shutdown.

[74] The geometry of the ice plain makes it much less sensitive to changes in width than the case near UpB. From equation (9), the width of the ice plain would have to contract by over 400 m/yr to match the observed deceleration rates. This is in contrast to observations that suggest a slight widening [*Bindschadler and Vornberger*, 1998]. Thus, as on UpB, observations of widening run counter to the observed deceleration trend.

[75] As noted above, ice stream speed is sensitive to τ_d. Applying equation (9) with the ice plain parameters and $(\tau_d - \tau_b) = 1.45$ kPa yields $\dot{U}_{\tau_d} = -5.4$ m/yr^2 when $\dot{\tau}_d = -0.007$ kPa/yr. This translates into a relative thinning of just greater than 10 cm/yr over a distance of 100 km. *Bindschadler et al.* [1993] estimated a pattern of thickening and thinning over the ice plain with gradients of more than 1 m/yr over 100 km. Thus, evolution of τ_d provides a plausible explanation for the ice plain deceleration, either in isolation or in conjunction with changes in τ_b as discussed next.

[76] Figure 8b shows curves of m_r, U, and $\dot{U}_{\tau_b}$ for the ice plain. The three sets of curves correspond to τ_d values of 2.8, 3.0, and 3.2 kPa. The curves reveal a strong sensitivity of m_r, U, and $\dot{U}_{\tau_b}$ to τ_d. In the absence of measurements of the basal temperature gradient on the ice plain, we assumed a value of $\Theta_b = 0.046$°C/m, which is the value needed to match the observations as discussed below. This value is close to that obtained using the local accumulation rate of 10 cm/yr in equation (2). At UpB, however, the best fit to the measured temperature profile (rms residual error 0.1°C) is achieved with an "effective" accumulation rate of 15 cm/yr. If this "effective" value is applicable to the ice plain, then $\Theta_b = 0.051$°C/m. Ice from Ice Stream A and Whillans B1, however, originates farther inland so even steeper gradients are plausible. As a result, Θ_b is poorly constrained on the ice plain by existing measurements.

[77] The velocity curves suggest that at the observed velocities of roughly 400 m/yr, the ice plain operates in the unstable region of the undrained plastic bed model. The $\dot{U}_{\tau_b}$ curves in Figure 8b indicate that the velocity-driven thermal evolution of the bed can lead to deceleration rates of

5 m/yr. This is largely a consequence of our selection of $\Theta_b = 0.046$°C/m, which was chosen to roughly match the observed deceleration rates. Within a reasonable adjustment of the model parameters (e.g., G, B, and τ_d), the observed deceleration can be matched over a range of τ_b values.

[78] We can examine the potential for ice stream stability by comparing conditions on the ice plain with those at UpB. Using equation (5), the condition for zero melt rate is

$$\tau_b = \frac{k_i \Theta_b - G}{U_b}. \quad (14)$$

Both areas move at about 400 m/yr. To simplify the argument we assume $\Theta_b = 0.046$°C/m for both cases, which is a little high for UpB and perhaps low for the ice plain. In both cases, with $G = 0.07$ W/m^2, $\tau_b = 2.1$ kPa is required to maintain $m_r = 0$. Maximum melt occurs where $\tau_b = 0.25\tau_d$ [*Raymond*, 2000]. On plots such as those in Figure 8, the stable $m_r = 0$ point lies to the left of this value and the unstable $m_r = 0$ point lies to the right. For UpB with $\tau_d \approx 12$ kPa, maximum melt is achieved at $\tau_b = 3$ kPa, so that with $\tau_b = 2.1$ kPa the stable $m_r = 0$ point is readily achieved. In contrast, with $\tau_d \approx 3$ kPa, a basal stress of $\tau_b = 2.1 > 0.25\tau_d$ kPa yields an unstable $m_r = 0$ point for the ice plain of Whillans Ice Stream.

[79] If we vary the velocity in equation (14), then the ice plain requires speeds well in excess of 1000 m/yr to operate at the stable $m_r = 0$ point. Such speeds for an ice stream 120 km wide are unsustainable due to mass balance considerations. If the geometry of the ice stream were to evolve toward a higher τ_d, then τ_b would have to increase accordingly to maintain a sustainable velocity and the stable $m_r = 0$ condition could still not be met. If τ_d were smaller, extreme velocities are still required to avoid basal freezing. If the margins are weakened by strain rate enhancement, then the trend is toward even larger velocities near the stable point. Thus, under undrained conditions, once an ice stream reaches a certain width, there is no way to reach the stable region of the model and maintain mass balance. Similar conclusions can be drawn from more detailed numerical modeling [*Bougamont et al.*, 2002].

[80] If we allow drainage to occur, then we need to replace m_r with $m_r - d_r$. A net drainage yields $m_r - d_r$ curves similar in form to the mr curves in Figure 8, except shifted down along the *y axis*. This makes it even more difficult to achieve stable conditions as greater melting is required. Import of water ($d_r < 0$) has the effect of shifting the curves up. This forces the stable $m_r - d_r = 0$ point to smaller τ_b than for undrained conditions. With such a small τ_b, the ice plain would require $\tau_d \approx 1.4$ kPa to reach a velocity that keeps it in balance. While with water import this is possible, the force balance results for the current ice plain geometry yield values of τ_b and τ_d that suggest that it is near the unstable point with relatively little water drainage or import. Similar conclusions can be drawn for a range of drainage conditions as considered qualitatively by *Raymond* [2000]. We note that most outlet glaciers operate in the drainage limited (unstable) regime. In general, however, with more efficient drainages and a lack of till, the basal resistance of such "hard-bedded" glaciers does not have such strong sensitivity to melt rate or tendency toward instability.

[81] With the data in hand, there is too little constraint on the model parameters to be able to determine precisely whether the ice plain slowdown on Whillans Ice Stream is entirely due to changes in τ_b and the thermal evolution of an undrained plastic bed. The important point is that a significant sector of the parameter space of the model is consistent with the observed rates of deceleration. The conclusion that the ice plain operates in the unstable regime is robust over an even wider range of model parameters. This is in contrast to the UpB case where no reasonable adjustment of the model parameters leads to values of $\dot{U}_{\tau_b}$ that are close to observed deceleration rates or that cause a shift into the unstable regime. Thus, the plastic bed model provides a plausible explanation for the ice plain deceleration.

[82] The discussion above identifies both changes in driving stress and the strengthening of a plastic bed as possible causes for the observed deceleration. There are additional feedbacks that we have not explored. For example, deceleration due to reduction in τ_d should decrease basal melting to further strengthen the bed and cause additional deceleration. These factors could combine in ways that either promote or impede stability. A more detailed understanding of the evolution of the ice plain requires more sophisticated models that include these feedbacks. In addition, these models should take into account the full spatial pattern of thickness change. Such models also need to be better constrained by new field measurements of Θ_b, B, G, till properties, and by remotely sensed measurements of the patterns of thickness and velocity change.

6.4.3. Ice Stream C

[83] Flow in the main body of Ice Stream C was initially estimated to have shutdown 140–150 years ago [*Retzlaff and Bentley*, 1993; *Anandakrishnan et al.*, 2001]. As revealed earlier by field measurements [*Bell et al.*, 1998] and previous SRI velocity data [*Joughin et al.*, 1998], the data in Figure 1 indicate that much of the upstream area of Ice Stream C is still active and is fed by an extensive tributary network. The active parts of the ice stream move at about 60–70 m/yr. The presence of buried crevasses along the shear margins in the active regions [*Retzlaff and Bentley*, 1993; *Smith*, 1999], indicates that significantly faster flow occurred in the past. A bulge is growing at the transition from active to stagnant flow with inferred thickening rates of more than 1 m/yr [*Alley et al.*, 1994; *Joughin et al.*, 1999; *Price et al.*, 2001].

[84] The force balance results (Table 3) indicate that lateral drag balances only about 25% of the driving stress on the active portion of Ice Stream C, indicating a significantly stronger bed (11.3 kPa) than beneath Ice Stream A and Whillans Ice Stream. Tests on till samples from UpC boreholes [*Kamb*, 2001] are consistent with a plastic bed model [*Tulaczyk et al.*, 2000b]. When the till behaves in a plastic manner, only 20 cm of water needs to be removed from a 6 m thick layer of till to increase the bed strength from 2 to 12 kPa. As a result, a 1.3 mm/yr freeze-on rate over a 150 year period could change till strength from that beneath active ice streams [*Kamb*, 2001] to the value of 11.3 kPa that we estimate. Farther downstream at the UpC camp where the ice is nearly stagnant, a basal temperature gradient of 0.052°C/m was measured [*Kamb*, 2001], leading to a freeze-on rate of 4.1 mm/yr for a geothermal heat flux of 0.07 W/m^2. Recent borehole observations of layered, debris-rich

basal ice in the nearly stagnant UpC area are consistent with the occurrence of basal freeze-on in the recent past (Engelhardt and Kamb, personal communication, 2001).

[85] As just described, till consolidation due to basal freezing provides a feasible explanation for the calculated high value of basal shear stress. However, there are no borehole or geophysical observations from this area on Ice Stream C that could be used to either confirm or deny the importance of basal freeze-on. We acknowledge that other explanations, such as the existence of sticky spots [*Alley*, 1993], are equally admissible. It is worthwhile to note that this part of Ice Stream C is located over relatively deep subglacial basins, similar to those underlying many ice–stream tributaries. Hence, the bed of this part of the ice stream for which we calculate the force balance may be more similar in its physical nature to the beds of ice stream tributaries, for which we consistently derive high basal shear stresses.

[86] The ice in the active region is significantly thicker (1400–2000 m) than in the stagnant region (600–1200 m), which will influence the basal melt rate. We estimated basal melt rate using equation (5). Basal shear heating was determined using $\tau_b = 11.3$ kPa (Table 3) and the velocity data. We used equation (2) to estimate temperature profiles from which we derived the basal temperature gradient. When the local accumulation rate (10.6 cm/yr ice equivalent) [*Giovinetto and Bentley*, 1985] is used in equation (2), it provides a poor fit to the measured temperature profile from the UpC camp (Engelhardt and Kamb, personal communication). A much better fit (rms residual of 0.74°C) is obtained if we use an ''effective'' accumulation rate of 28.5 cm/yr. The need for an effective value to obtain a good match may reflect the fact that the tributaries feeding UpC draw ice relatively rapidly from near the ice divide, where surface temperatures are colder and accumulation is higher. A sustained period of thinning with consequent downward advection could also contribute to the larger effective accumulation rate.

[87] We assume that the local accumulation rate yields an upper bound on basal melt rate estimates, while the UpC effective accumulation rate provides a lower bound. With the effective accumulation rate, the basal melt/freeze transition is located where the ice is ~1700 m thick on the active portion of Ice Stream C, which is at about 730 m elevation (Figure 3). Using the local accumulation rate, the basal melt/freeze transition corresponds to an ice thickness of ~1250 m, which is just below the 600 m surface elevation contour (Figure 3). The melt rates based on the effective accumulation rate yield freeze-on rates of roughly 0–2 mm/yr over portions of the active region, which may have strengthened the bed and slowed the ice stream. The upper and lower bounds on the location of the melt/freeze transition also contain the current stagnation front. This means that ice may continue to flow in the active portions of Ice Stream C because the thicker ice there provides a warmer bed that either maintains melting or reduces freezing to a level where full stagnation has yet to occur or will not occur. It is difficult to tell whether a steady state has been reached or a strengthening of the bed is ongoing.

6.4.4. Ice Plain of Ice Stream C

[88] Ice Stream C has an ice plain (area below 200 m contour in Figure 3) with similar geometry to that of Whillans Ice Stream. We believe that the shutdown of Ice Stream C likely began due unstable ice plain behavior and strengthening of a plastic bed similar to that which may be causing the current deceleration on Whillans Ice Stream. Recent numerical modeling of the stoppage of Ice Stream C also indicates that freeze-on-driven stoppage of the ice stream begins near its grounding line but propagates very fast (over several decades) through all of the ice stream trunk (Bougamont et al., submitted manuscript, 2002). Both ice plains have similar geometry and would be expected to undergo similar thermal evolution. If Whillans Ice Stream is indeed shutting down, the shutdowns of these ice streams would be nearly simultaneous on a glacial–interglacial timescale. In the remainder of this section we examine evidence that supports our conclusion that the stagnation initiated on the ice plain and migrated upstream.

[89] If the ice plain shut down first, it would dam the ice behind it, causing the dammed ice to slow down. This reduction in speed would likely decrease basal melt or initiate basal freezing to yield further stagnation, resulting in an upstream propagation of the stagnation front. A bulge is currently forming due to compressional thickening just above the current stagnation front [*Alley et al.*, 1994; *Joughin et al.*, 1999; *Price et al.*, 2001]. The bulge formation has the effect both of steepening the ice along the stagnation front and of raising the central portion of the stream relative to the margins. As a result, just above and below the 600 m elevation contour (Figure 3) the two branches of ice stream are raised with respect to the slow spot separating them [*Price et al.*, 2001]. In contrast, the elevation of the Unicorn, the ridge separating Whillans B1 and B2, is well above that of the surrounding ice streams. There is also a slow spot, near the UpC camp at roughly 500 m elevation. This spot is also lower with respect to the central parts of the ice stream, suggesting that this too was once a region of active deceleration and bulge formation. These observations suggest an upstream progression of the stagnation front that passed through the UpC region on route to its present location. This runs counter to the hypothesis of *Alley et al.* [1994] that the wave of stagnation propagated down-glacier, but is consistent with the initial conclusion of an upstream migration by *Retzlaff and Bentley* [1993].

[90] The area between the 600 and 200 m contours appears to be oversteepened with respect to the other ice streams. The average driving stress between these contours is 22 ± 2 kPa, which is significantly larger than that found on the active regions of the other ice streams (see Table 3). This oversteepened ice may be the result of thickening following stagnation. It is likely that the current flux (12.2 km^3/yr) through the gate at the upper end of Ice Stream C (blue line in Figure 3) is similar to or less than the average flux over the last 150 years. With negligible flux across the grounding line, this means that roughly 1830 km^3 of ice must have contributed to a thickening of the ice stream following stagnation. If the ice plain stopped relatively quickly, most of this thickening should have occurred at or below the region of current thickening and above the ice plain as indicated by the purple outline in Figure 3. The area of this region is 19,200 km^2, which yields an average total thickening of 96 m. If thickening increased linearly from zero above the ice plain to a maximum at the region just

above the current stagnation front, this would yield a thickening of the upstream region by nearly 200 m. Although the region we chose could be drawn differently, the fact remains that there is a substantial volume of ice available for thickening since stagnation [*Alley et al.*, 1994]. Steepening and thickening of the ice behind the ice plain is consistent with an initial shutdown on the plain followed by an upstream retreat of the stagnation front.

[91] An upstream migration and thickening above the ice plain as we have described is not inconsistent with data that have been used to suggest a nearly synchronous shutdown [*Anandakrishnan et al.*, 2001]. There is a slight trend toward younger buried crevasses toward the upstream regions of C, suggesting some upstream migration [*Smith*, 1999; *Retzlaff and Bentley*, 1993]. The errors (±10 to 30 years) are also large enough to allow additional time for upstream migration. Furthermore, the presence of buried crevasses does not indicate complete stagnation, but rather a decrease in speed to a level below about 120 m/yr, which is the minimum value needed to maintain crevassing [*Scambos and Bindschadler*, 1993]. The current region of bulge growth and active flow lies in an area where buried crevasses would otherwise suggest a shutdown over a century ago. Consequently, bulge formation could have occurred near UpC well after active crevassing along the margins ceased. Finally, a roughly linear thickening trend as described earlier implies an inland migration rate with diminishing speed as suggested by *Retzlaff and Bentley* [1993].

[92] There is other evidence suggesting that the shutdown may have initiated on the ice plain. Satellite image data indicate an undated rapid inward migration of the margin along ridge B/C and radar echo-sounding data indicate that a jump in the northern margin, the "duck foot," occurred roughly 300–500 years ago [*Jacobel et al.*, 2000]. Together these represent a narrowing of the width of the ice plain by roughly 40% and indicate unstable behavior on the ice plain prior to stagnation. This narrowing should have caused a reduction in speed, which perhaps ultimately altered the basal melt rates at the bed leading to the shutdown. Alternatively, a reduction in speed due to the widening may have reduced thinning or caused thickening to allow continued motion for an additional 2 to 3 centuries.

[93] As just described, we believe that the shutdown initiated on the ice plain and was likely caused by the strengthening of a weak plastic bed as water was removed by basal freezing. Although the direction of propagation of the stagnation front that we suggest is the opposite of that originally postulated in the water piracy theory [*Alley et al.*, 1994], our conclusions are not inconsistent with water piracy. If we relax the assumption of undrained conditions, then the ice plain of Ice Stream C is thin enough that it may have required the import of water from upstream as has been postulated for the ice plain of Whillans Ice Stream [*Raymond*, 2000]. Any diversion (water piracy) of basal water flow from upstream could have initiated the shutdown by allowing basal freeze-on to overcome water import, which would withdraw water from the till, strengthen it, and initiate stagnation. This shutdown likely would have begun on the ice plain, where the ice is the thinnest and conditions most favor basal freeze-on. If water piracy did divert additional water to Whillans Ice Stream, then this raises the question of why, despite the additional water, is it slowing down in a way that appears similar to the slowdown of Ice Stream C.

6.4.5. Ice Stream D

[94] The velocity profiles in Figure 6 indicate that Ice Stream D moves at roughly 400 m/yr, which is comparable to speeds on much of Whillans Ice Stream and Ice Stream E. With a width of 55 km, it is wider than all active streams except the ice plain of Whillans Ice Stream and Ice Stream E. Lateral drag is estimated to support just over half of the driving stress (Table 3). This yields an estimate of $\tau_b = 4.7$ kPa with an uncertainty of 0.8 kPa. This relatively low uncertainty is the result of the availability of satellite altimeter data with which to estimate τ_d. This uncertainty, however, represents statistical variability in the data and does not include assumptions about the flow law.

[95] *Raymond* [2000] estimated basal drag on Ice Stream D with flow-law parameters corresponding to ice at $-9°C$ and a spatially dependent enhancement factor that ranged from 10 at the margin to 1 at the centerline. This flow-law parameterization yields estimates of τ_b ranging from 6 to 10 kPa, which likely represents an upper bound on τ_b. Laboratory tests on ice recovered from the shear margin near UpB yield a maximum marginal shear stress of 260 kPa. If conditions are similar for both ice streams, this leads to an approximate lower bound of $\tau_b = 1.6$ kPa for $\tau_d = 10$ kPa. Tests of till strength from samples recovered from boreholes on Ice Stream D yield local values of $\tau_b = 1$ kPa [*Kamb*, 2001], which is significantly smaller than both our estimate of 4.7 kPa and the approximate lower bound of 1.6 kPa. This difference might be the result of a bed that is strengthened by the presence of "sticky spots" [*Alley*, 1993] due to a patchy or uneven distribution of till or till water content. The UpD camp is located in an area where the ice stream is much narrower than our sampling region, so the smaller value of τ_b found there may reflect a greater lateral resistance.

[96] Studies at UpB [*Jackson and Kamb*, 1997; *Harrison et al.*, 1998] indicate that there is little enhancement to the flow law at the margins. Our results near UpB are consistent with those of earlier studies [*Jackson and Kamb*, 1997; *Whillans and Van der Veen*, 1997; *Harrison et al.*, 1998]. If similar conditions apply at the margins of Ice Stream D, then our estimate, while still subject to some uncertainty, is probably not biased significantly high or low by our choice of flow-law parameters and assumption of no flow-law enhancement. This suggests that τ_b is significantly greater for Ice Stream D (~4.7 kPa) than for Whillans Ice Stream (0–2 kPa).

[97] The basal shear stress determines the basal shear heating and, thus, the basal melt rate. Taking the measured value of $\Theta_b = 0.053°C/m$ [*Engelhardt and Kamb*, 1998], $G = 0.07$ W/m^2, and a speed of 400 m/yr, the bed may be either freezing (-3.0 mm/yr for $\tau_b = 1$ kPa) or melting (1.9 mm/yr for our estimate of 4.7 kPa, Table 4). Based on a limited comparison of velocities, there is no evidence from the data we have examined or other data sets (Scambos, personal communication, 2001) to suggest that Ice Stream D is slowing significantly. Therefore, we infer that Ice Stream D is in a stable mode of motion, either the unconditionally stable undrained mode or the drainage-regulated mode of *Raymond* [2000].

6.4.6. Ice Stream E

[98] Despite its great width of 78 km, Ice Stream E has a larger driving stress (15.3 kPa) than other ice streams moving at similar speed. The force balance results indicate that side drag supports just over 25% of the driving stress, leaving the bed to support the remaining 10.9 kPa. Even allowing for significant error in the flow-law parameterization, the bed of Ice Stream E appears to be significantly stronger than that of Whillans Ice Stream (0–2 kPa). Furthermore, the profiles of marginal shear stress shown in Figure 6, show a significant departure from the linear profiles expected for ice streams controlled largely by side shear.

[99] The velocity data for Ice Stream E show much more structure than for the other ice streams, particularly at wavelengths of 1–10 km. Significantly more structure is also visible in the SAR imagery of Ice Stream E than can be seen on many of the other ice streams. There are also several bumps visible in the surface topography. These observations suggest that bed topography plays a significant role in controlling flow in the ice stream. Unfortunately, the bed topography data for Ice Stream E (Figure 4) were derived from a significantly sparser data set than many areas on other ice streams. Thus, is difficult to determine whether Ice Stream E has a significantly rougher bed.

[100] Bed topography will have an influence on basal resistance. First, high spots protruding above the marine sediment drape would increase bed resistance by providing unlubricated sticky spots. Second, even in the case of a perfectly lubricated bed, significant topography would resist flow through form drag [*Van der Veen*, 1999; *Gudmundsson et al.*, 1998]. Whatever the influence of topography, Ice Stream E would have to slow down to 120 m/yr for basal freezing to begin, assuming $\Theta_b = 0.053$°C/m (Ice Stream D value), $G = 0.07$ W/m^2, and the estimated τ_b.

6.5. Paleo Ice Streams

[101] The mechanisms responsible for ice plain instability may also have played a role in the retreat of "paleo ice streams." At the last glacial maximum, the area now occupied by the Ross Ice Shelf was grounded and the grounded ice sheet extended out to the edge of the continental shelf [*Anderson and Shipp*, 2001]. This ice sheet was drained by several paleo ice streams, which were extensions of the present ice streams [*Anderson and Shipp*, 2001]. These ice streams appear to have had large widths (up to ~100 km). Ice cores indicate that the elevation at Siple Dome has not changed by more than a few hundred meters over the last glacial cycle [*Steig et al.*, 2001]. This suggests a relatively flat ice sheet with low (e.g., several kPa) driving stresses out to the grounding line. These ice streams are believed to have been underlain by a layer of soft, deformable till [*Anderson and Shipp*, 2001; *Domack et al.*, 1999]. Thus, the paleo ice streams may have had weak beds and similar geometries (flat, wide, and thin) to the ice plains of Whillans Ice Stream and Ice Stream C.

[102] At sustainable speeds (e.g., near the balance velocities), ice plains or flat, wide ice streams tend to operate near the unstable point of the plastic bed model. In the discussion above we have focused mainly on the instability that drives such an ice stream toward shutdown. At positive melt rates, however, this can lead to a trend toward increasing speed and overthinning. Although we have suggested that such overthinning can perhaps lead to shutdown, it is also possible that rapid thinning can lead to ungrounding before freezing at the bed initiates. In this case, the instability provides a mechanism for grounding line retreat, which might help explain the large grounding-line retreat rates of up to 1300 km that have taken place since the last glacial maximum [*Conway et al.*, 1999]. Although this grounding-line retreat has been attributed to rising sea level [*Denton and Hughes*, 1986], recent evidence shows that the ice sheet did not lose contact with its bed in a direct response to rising sea level [*Anderson and Shipp*, 2001]. Furthermore, the seafloor evidence indicates that the ice streams behaved independently [*Anderson and Shipp*, 2001], suggesting the retreat of each was driven by its own dynamics.

7. Summary

[103] Using satellite radar interferometry, we have produced a velocity map that covers much of the Siple Coast ice streams. This is the most comprehensive velocity mapping of this area. Error estimates and comparison with field measurements indicate that the accuracy of the data is better than 5 m/yr over most of the map.

[104] Our comparison with measurements from the mid 1970s and 1980s confirms earlier estimates of deceleration on Whillans Ice Stream and also suggests a slowdown on Ice Stream A. We find that the ice plain of Whillans Ice Stream is slowing at annual rate of 5.5 m/yr^2.

[105] We have applied standard force balance techniques to areas on both the ice streams and the tributaries that feed them. Typical basal shear stresses on the tributaries range from about 15 to 25 kPa, which corresponds to about half the driving stress. Higher basal shear stresses beneath tributaries suggest melt rates of several millimeters per year at typical tributary speeds. Comparison with the bed topography reveals that the tributaries feeding the ice streams coincide well with a network of subglacial valleys, indicating that, unlike the ice streams, they are strongly influenced by subglacial topography.

[106] We have examined the sensitivity of ice streamflow to various controlling parameters. We find that deceleration at the UpB camp is consistent with a decrease in driving stress over time. In contrast, the ice plain appears to operate in an unstable regime of the plastic bed model so that a strengthening of the bed may be responsible for the deceleration. A decrease in driving stress could also be responsible, indicating that further data and more sophisticated models are needed to resolve the exact source of deceleration. Nevertheless, our results suggest that ice plains or fast, wide ice streams underlain by a plastic till bed are inherently unstable. This conclusion is consistent with inferences of unstable flow over the last 1000 years [*Fahnestock et al.*, 2000].

[107] Analysis of Ice Stream C suggests that the active portions of the stream coincided well with the area where there is melting or the basal freezing rates are small. The current stagnation front roughly coincides roughly with the transition from basal freezing to melting. This suggests that local thermodynamic conditions at the bed may play a role in determining the transition from active to stagnant flow. We hypothesize that a shutdown on the ice stream occurred due to the unstable nature of the ice plain and possibly in a manner consistent with the current deceleration on the Ice

Plain of Whillans Ice Stream. The current topography and bulge thickening are consistent with an upstream retreat initiated on the ice plain.

[108] On Ice Stream D there is enough uncertainty in the basal shear-stress estimates that it is difficult to determine whether melting or freezing is occurring at the bed. Its fast motion and apparent lack of temporal variation in speed argue in favor of some basal melt. In contrast, even with a large uncertainty, basal resistance on Ice Stream E is large enough that basal melt must be taking place. Subglacial topography or other conditions act to strengthen the bed and promote the stability of this ice stream despite its great width.

[109] **Acknowledgments.** I. Joughin performed his contribution to this work at the Jet Propulsion Laboratory, California Institute of Technology, under contract with NASA. S. Tulaczyk was funded under by the National Science Foundation (NSF-OPP-0096302). R. Bindschadler and S. Price were funded by NASA under NRA-98-OES-3. The RADARSAT data were acquired by the Canadian Space Agency and were downlinked and processed to L0-products by the Alaska SAR Facility. Mosaicked RADARSAT images and the surface DEM were provided by K. Jezek of the Byrd Polar Research Center. D. G. Vaughan and the BEDMAP project produced the bed topography DEM. Many of the data sets we used were archived at the National Snow and Ice Data Center. Discussions with C. Hulbe improved the content of this manuscript and R. Alley and the Associate Editor's comments resulted in significant improvements to the manuscript.

References

Alley, R. B., In search of ice-stream sticky spots, *J. Glaciol.*, *39*(133), 447–454, 1993.

Alley, R. B., and R. A. Bindschadler, The West Antarctic Ice Sheet and sea-level change, *AGU Antarct. Res. Ser.*, *77*, 1–11, 2001.

Alley, R. B., D. D. Blankenship, C. R. Bentley, and S. T. Rooney, Till beneath Ice Stream-B, 3, Till deformation: Evidence and implications, *J. Geophys. Res.*, *92*(B9), 8921–8929, 1987.

Alley, R. B., D. D. Blankenship, S. T. Rooney, and C. R. Bentley, Sedimentation beneath ice shelves: The view from Ice Stream-B, *Mar. Geol.*, *85*, 101–120, 1989.

Alley, R. B., S. Anandakrishnan, C. R. Bentley, and N. Lord, A water piracy hypothesis for the stagnation of Ice Stream C, Antarctica, *Ann. Glaciol.*, *20*, 187–194, 1994.

Anandakrishnan, S., D. D. Blankenship, R. B. Alley, and P. A. Stoffa, Influence of subglacial geology on the position of a West Antarctica ice stream from seismic measurements, *Nature*, *394*, 62–65, 1998.

Anandakrishnan, S., R. B. Alley, R. W. Jacobel, and H. Conway, The flow regime of Ice Stream C and hypotheses concerning its recent stagnation, *AGU Antarct. Res. Ser.*, *77*, 283–296, 2001.

Anderson, J. B., and S. S. Shipp, Evolution of the West Antarctic Ice Sheet, *AGU Antarct. Res. Ser.*, *77*, 45–57, 2001.

Bamber, J. L., and R. A. Bindschadler, An improved elevation dataset for climate and ice-sheet modelling: Validation with satellite imagery, *Ann. Glaciol.*, *25*, 438–444, 1997.

Bell, R. E., D. D. Blankenship, C. A. Finn, D. L. Morse, T. A. Scambos, J. M. Brozena, and S. M. Hodge, Influence of subglacial geology on the onset of a West Antarctic ice stream from aerogeophysical observations, *Nature*, *394*(6688), 58–62, 1998.

Bindschadler, R., and P. Vornberger, Changes in the West Antarctic Ice Sheet since 1963 from declassified satellite photography, *Science*, *279*, 689–692, 1998.

Bindschadler, R., P. L. Vornberger, and S. Shabtaie, The detailed net mass-balance of the Ice plain on Ice Stream-B, Antarctica: A geographic information-system approach, *J. Glaciol.*, *39*(133), 471–482, 1993.

Bindschadler, R., P. Vornberger, D. Blankenship, T. Scambos, and R. Jacobel, Surface velocity and mass balance of Ice Streams D and E, West Antarctica, *J. Glaciol.*, *42*(142), 461–475, 1996.

Bindschadler, R., J. Bamber, and S. Anandakrishnan, Onset of streaming flow in the Siple Coast Region, *AGU Antarct. Res. Ser.*, *77*, 123–136, 2001.

Blankenship, D. D., C. R. Bentley, S. T. Rooney, and R. B. Alley, Till beneath Ice Stream-B, 1, Properties derived from seismic travel-times, *J. Geophys. Res.*, *92*(B9), 8903–8911, 1987.

Blankenship, D. D., D. L. Morse, C. A. Finn, R. E. Bell, M. E. Peters, S. D. Kempf, S. M. Hodge, M. Studinger, J. C. Behrendt, and J. M. Brozena, Geologic controls on the initiation of rapid basal motion for West Antarctic Ice Streams, *AGU Antarct. Res. Ser.*, *77*, 105–122, 2001.

Bougamont, M., S. Tulaczyk, and I. Joughin, Response of subglacial sediments to basal freeze-on, 2, Application in numerical modeling of the recent stoppage of Ice Stream C, West Antarctica, *J. Geophys. Res.*, *107*, doi:10.1029/2002JB001936, in press, 2002.

Chen, X., R. A. Bindschadler, and P. L. Vornberger, Determination of velocity field and strain rate field in West Antarctica using high precision GPS measurements, in *Survey. Land Inf. Syst.*, *48*, 247–255, 1998.

Conway, H., B. L. Hall, G. H. Denton, A. M. Gades, and E. D. Waddington, Past and future grounding-line retreat of the West Antarctic Ice Sheet, *Science*, *286*, 280–283, 1999.

Cuffey, K., and R. Alley, Is erosion by deforming subglacial sediments significant? (Toward till continuity), *Ann. Glaciol.*, *22*, 126–133, 1996.

Denton, G. H., and T. J. Hughes, Global ice-sheet system interlocked by sea level, *Quat. Res.*, *26*(1), 3–26, 1986.

Domack, E. W., E. A. Jacobson, S. Shipp, and J. B. Anderson, Late Pleistocene–Holocene retreat of the West Antarctic Ice-Sheet system in the Ross Sea, part 2, Sedimentologic and stratigraphic signature, *Geol. Soc. Am. Bull.*, *111*(10), 1517–1536, 1999.

Echelmeyer, K. A., W. D. Harrison, C. Larsen, and J. E. Mitchell, The role of the margins in the dynamics of an active ice stream, *J. Glaciol.*, *40*(136), 527–538, 1994.

Echelmeyer, K. A., and W. D. Harrison, Ongoing margin migration of Ice Stream B, Antarctica, *J. Glaciol.*, *45*(150), 361–369, 1999.

Engelhardt, H., and B. Kamb, Vertical temperature profile of ice stream B, *Antarct. J. U. S.*, *28*, 63–66, 1993.

Engelhardt, H., and B. Kamb, Basal hydraulic system of a West Antarctic ice stream: Constraints from borehole observations, *J. Glaciol.*, *43*(144), 207–230, 1997.

Engelhardt, H., and B. Kamb, Thermal history of the West Antarctic Ice Sheet, paper presented at The West Antarctic Ice Sheet Chapman Conference, Orono, Maine, 13–18 September 1998.

Fahnestock, M. A., T. A. Scambos, R. A. Bindschadler, and G. Kvaran, A millenium of variable ice flow recorded by the Ross Ice Shelf, Antarctica, *J. Glaciol.*, *46*(155), 652–664, 2000.

Giovinetto, M. B., and C. R. Bentley, Surface balance in ice drainage systems of Antarctica, *Antarct. J. U. S.*, *20*, 6–13, 1985.

Giovinetto, M. B., N. M. Waters, and C. R. Bentley, Dependence of Antarctic surface mass balance on temperature, elevation, and distance to open ocean, *J. Geophys. Res.*, *95*(D4), 3517–3531, 1990.

Goldstein, R. M., Atmospheric limitations to repeat-track radar interferometry, *Geophys. Res. Lett.*, *22*(18), 2517–2520, 1995.

Gray, A. L., K. E. Mattar, and G. Sofko, Influence of ionospheric electron density fluctuations on satellite radar interferometry, *Geophys. Res. Lett.*, *27*(10), 1451–1454, 2000.

Gudmundsson, G. H., C. F. Raymond, and R. Bindschadler, The origin and longevity of flow stripes on Antarctic ice streams, *Ann. Glaciol.*, *27*, 145–152, 1998.

Hamilton, G. S., I. M. Whillans, and P. J. Morgan, First point measurements of ice-sheet thickness change in Antarctica, *Ann. Glaciol.*, *27*, 125–129, 1998.

Harrison, W. D., K. A. Echelmeyer, and C. F. Larsen, Measurement of temperature in a margin of Ice Stream B, Antarctica implications for margin migration and lateral drag, *J. Glaciol.*, *44*(148), 615–624, 1998.

Hodge, S. M., and S. K. Doppelhammer, Satellite imagery of the onset of streaming flow of Ice Streams C and D, West Antarctica, *J. Geophys. Res.*, *101*(C3), 6669–6677, 1996.

Hulbe, C. L., and I. M. Whillans, Weak bands within Ice Stream B, West Antarctica, *J. Glaciol.*, *43*(145), 377–386, 1997.

Hulbe, C. L., I. R. Joughin, D. L. Morse, and R. A. Bindschadler, Tributaries to West Antarctica ice streams: Characteristics deduced from numerical modeling of ice flow, *Ann. Glaciol.*, *31*, 184–190, 2000.

Jackson, M., and B. Kamb, The marginal shear stress of Ice Stream B, West Antarctica, *J. Glaciol.*, *43*(145), 415–426, 1997.

Jacobel, R. W., T. A. Scambos, N. A. Nereson, and C. F. Raymond, Changes in the margin of Ice Stream C, Antarctica, *J. Glaciol.*, *46*(152), 102–110, 2000.

Jezek, K. C., Glaciological properties of the Antarctic ice sheet from RADARSAT-1 synthetic aperture imagery, *Ann. Glaciol.*, *29*, 286–290, 1999.

Joughin, I., Ice sheet velocity mapping: A combined interferometric and speckle tracking approach, *Ann. Glaciol.*, *34*, 195–201, 2002.

Joughin, I., and S. Tulaczyk, Positive mass balance of the Ross Ice Streams, West Antarctica, *Science*, *295*, 476–480, 2002.

Joughin, I., R. Kwok, and M. Fahnestock, Interferometric estimation of three-dimensional ice-flow using ascending and descending passes, *IEEE Trans. Geosci. Remote Sens.*, *36*(1), 25–37, 1998.

Joughin, I., L. Gray, R. Bindschadler, S. Price, D. Morse, C. Hulbe, K. Mattar, and C. Werner, Tributaries of West Antarctic ice streams revealed by RADARSAT interferometry, *Science*, *286*, 283–286, 1999.

Kamb, B., Rheological nonlinearity and flow instability in the deforming-bed mechanism of ice stream motion, *J. Geophys. Res.*, *96*(B10), 16,585–16,595, 1991.

Kamb, B., Basal zone of the West Antarctic Ice Streams and its role in lubrication of their rapid motion, *AGU Antarct. Res. Ser.*, *77*, 157–200, 2001.

Liu, H., K. Jezek, and B. Li, Development of Antarctic digital elevation model by integrating cartographic and remotely sensed data: A geographic information system based approach, *J. Geophys. Res.*, *104*(B10), 23,199–23,213, 1999.

Liu, H., K. Jezek, and B. Li, *Radarsat Antarctic Mapping Project Digital Elevation Model*, Natl. Snow and Ice Data Cent., Boulder, Colo., 2000.

Lythe, M. B., and D. G. Vaughan, BEDMAP: A new ice thickness and subglacial topographic model of Antarctica, *J. Geophys. Res.*, *106*(B6), 11,335–11,351, 2001.

McIntyre, N. F., The dynamics of ice-sheet outlets, *J. Glaciol.*, *31*(108), 1985.

Mercer, J. H., Antarctic ice and Sangamon sea-level rise, *IAHS Publ.*, *179*, 217–225, 1968.

Michel, R., and E. Rignot, Flow of Glacier Moreno, Argentina, from repeat-pass Shuttle Imaging Radar images: Comparison of the phase correlation method with radar interferometry, *J. Glaciol.*, *45*(149), 93–102, 1999.

Mohr, J. J., N. Reeh, and S. N. Madsen, Three-dimensional glacial flow and surface elevation measured with radar interferometry, *Nature*, *391*, 273–276, 1998.

Paterson, W. S. B., *The Physics of Glaciers*, 3rd Ed., 480 pp., Pergamon, New York, 1994.

Price, S. F., and I. M. Whillans, Delineation of a catchment boundary using velocity and elevation measurements, *Ann. Glaciol.*, *27*, 140–144, 1998.

Price, S. F., R. A. Bindschadler, C. L. Hulbe, and I. R. Joughin, Post-stagnation behavior in the upstream regions of Ice Stream C, West Antarctica, *J. Glaciol.*, *47*(157), 283–294, 2001.

Raymond, C. F., Shear margins in glaciers and ice sheets, *J. Glaciol.*, *42*(140), 90–102, 1996.

Raymond, C. F., Energy balance of ice streams, *J. Glaciol.*, *46*(155), 665–674, 2000.

Raymond, C. F., K. A. Echelmeyer, I. M. Whillans, and C. S. M. Doake, Ice stream shear margins, *AGU Antarct. Res. Ser.*, *77*, 137–156, 2001.

Retzlaff, R., and C. R. Bentley, Timing of stagnation of Ice Stream C, West Antarctica, from short- pulse radar studies of buried surface crevasses, *J. Glaciol.*, *39*(133), 552–561, 1993.

Retzlaff, R., N. Lord, and C. R. Bentley, Airborne-radar studies: Ice Stream-A, Ice Stream-B and Ice Stream-C, West Antarctica, *J. Glaciol.*, *39*(133), 495–506, 1993.

Rooney, S. T., D. D. Blankenship, R. B. Alley, and C. R. Bentley, Till beneath Ice Stream-B, 2, Structure and continuity, *J. Geophys. Res.*, *92*(B9), 8913–8920, 1987.

Scambos, T. A., and R. A. Bindschadler, Complex ice stream flow revealed by sequential satellite imagery, *Ann. Glaciol.*, *17*, 177–182, 1993.

Smith, B., Radar studies on Ice Stream C, West Antarctica, Master's thesis, Univ. of Wis. Press, Madison, 15 December 1999.

Steig, E. J., J. L. Fastook, C. Zweck, I. D. Goodwin, K. J. Licht, J. C. White, and R. P. Ackert, West Antarctic ice sheet elevation changes, *AGU Antarct. Res. Ser.*, *77*, 75–90, 2001.

Stephenson, S. N., and R. A. Bindschadler, Observed velocity fluctuations on a major Antarctic ice stream, *Nature*, *334*, 695–697, 1988.

Studinger, M., R. E. Bell, D. D. Blankenship, C. A. Finn, R. A. Arko, D. L. Morse, and I. Joughin, Subglacial sediments: A regional geological template for ice flow in West Antarctica, *Geophys. Res. Lett.*, *28*(18), 3493–3496, 2001.

Thomas, R. H., D. R. MacAyeal, D. H. Eilers, and D. R. Gaylord, Glaciological studies on the Ross Ice Shelf, Antarctica, 1972–1978, The Ross Ice Shelf: Glaciology and geophysics, *AGU Antarct. Res. Ser.*, *42*, 21–53, 1984.

Tulaczyk, S., W. B. Kamb, and H. F. Engelhardt, Basal mechanics of Ice Stream B, West Antarctica, 1, Till mechanics, *J. Geophys. Res.*, *105*(B1), 463–481, 2000a.

Tulaczyk, S., W. B. Kamb, and H. F. Engelhardt, Basal mechanics of Ice Stream B, West Antarctica, 2, Undrained plastic bed model, *J. Geophys. Res.*, *105*(B1), 483–494, 2000b.

Tulaczyk, S., R. P. Scherer, and C. D. Clark, A ploughing model for the origin of weak tills beneath ice streams: A qualitative treatment, *Quat. Int.*, *86*, 58–70, 2001.

Van der Veen, C. J., *Fundamentals of Glacier Dynamics*, 462 pp., A. A. Balkema, Brookfield, Vt., 1999.

Whillans, I. M., Force budget of ice sheets, in *Dynamics of the West Antarctic Ice Sheet*, edited by C. J. Van der Veen and J. Oerlemans, pp. 17–36, D. Reidel, Norwell, Mass., 1987.

Whillans, I. M., and C. J. Van der Veen, New and improved determinations of velocity of Ice Streams B and C, West Antarctica, *J. Glaciol.*, *39*(133), 483–490, 1993.

Whillans, I. M., and C. J. Van der Veen, The role of lateral drag in the dynamics of ice stream B, Antarctica, *J. Glaciol.*, *43*(144), 231–237, 1997.

Whillans, I. M., J. Bolzan, and S. Shabtaie, Velocity of Ice Streams B and C, West Antarctica, *J. Geophys. Res.*, *92*(B9), 8895–8902, 1987.

Whillans, I. M., C. R. Bentley, and C. J. Van der Veen, Ice Streams B and C, *AGU Antarct. Res. Ser.*, *77*, 257–282, 2001.

Zotikov, I. A., *The Thermophysics Of Glaciers*, 275 pp., D. Reidel, Norwell, Mass., 1986.

R. Bindschadler, NASA Goddard Space Flight Center, Code 971, Greenbelt, MD 20771, USA. (bob@igloo.gsfc.nasa.gov)

I. Joughin, Jet Propulsion Laboratory, California Institute of Technology, M/S 300-235, 4800 Oak Grove Drive, Pasadena, CA 91109, USA. (ian@radar-sci.jpl.nasa.gov)

S. F. Price, Department of Earth and Space Sciences, University of Washington, Box 351650, Johnson Hall, Room 63, Seattle, WA 98195-1650, USA. (sprice@geophys.washington.edu)

S. Tulaczyk, Department of Earth Sciences, University of California-Santa Cruz, A208 Earth and Marine Sciences Building, Santa Cruz, CA 95064, USA. (tulaczyk@es.ucsc.edu)